

# On the HU Aquarii planetary system hypothesis

Krzysztof Goździewski<sup>1</sup>, İlham Nasiroğlu<sup>2,3</sup>, Aga Słowikowska<sup>4</sup>, Klaus Beuermann<sup>5</sup>, Gottfried Kanbach<sup>2</sup>, Bartosz Gauza<sup>6,7</sup>, Andrzej J. Maciejewski<sup>4</sup>, Robert Schwarz<sup>8</sup>, Axel D. Schwöpe<sup>8</sup>, Tobias C. Hinse<sup>9</sup>, Nader Haghighipour<sup>10</sup>, Vadim Burwitz<sup>2,11</sup>, Mariusz Słonina<sup>1</sup> and Arne Rau<sup>2</sup>

<sup>1</sup>Toruń Centre for Astronomy, Nicolaus Copernicus University, Gagarin Str. 11, 87-100 Toruń, Poland

<sup>2</sup>Max Planck Institute for Extraterrestrial Physics, Giessenbachstrasse, 85748 Garching, Germany

<sup>3</sup>University of Cukurova, Department of Physics, 01330 Adana, Turkey

<sup>4</sup>Kepler Institute of Astronomy, University of Zielona Góra, Lubuska 2, 65-265 Zielona Góra, Poland

<sup>5</sup>Universität Goettingen, Institut für Astrophysik, Friedrich-Hund-Platz 1, DE 37077 Göttingen, Germany

<sup>6</sup>Instituto de Astrofísica de Canarias (IAC), E-38200 La Laguna, Tenerife, Spain

<sup>7</sup>Dept. Astrofísica, Universidad de La Laguna (ULL), E-38206 La Laguna, Tenerife, Spain

<sup>8</sup>Leibniz-Institute für Astrophysik (AIP), An der Sternwarte 16, 14482 Potsdam, Germany

<sup>9</sup>Korea Astronomy and Space Science Institute (KASI), Optical Astronomy Research Center, 776 Daedukdae-ro, Daejeon, 305-348, Republic of Korea

<sup>10</sup>Institute for Astronomy and NASA Astrobiology Institute, University of Hawaii-Manoa, 2680 Woodlawn Drive, Honolulu, HI 96822, USA

<sup>11</sup>Observatorio Astronomico de Mallorca, 07144 Costitx, Mallorca, Spain

13 November 2018

## ABSTRACT

In this work, we investigate the eclipse timing of the polar binary HU Aquarii that has been observed for almost two decades. Recently, Qian et al. attributed large (O-C) deviations between the eclipse ephemeris and observations to a compact system of two massive jovian companions. We improve the Keplerian, kinematic model of the Light Travel Time (LTT) effect and re-analyse the whole currently available data set. We add almost 60 new, yet unpublished, mostly precision light curves obtained using the time high-resolution photo-polarimeter OPTIMA, as well as photometric observations performed at the MONET/N, PIRATE and TCS telescopes. We determine new mid-egress times with a mean uncertainty at the level of 1 second or better. We claim that because the observations that currently exist in the literature are non-homogeneous with respect to spectral windows (ultraviolet, X-ray, visual, polarimetric mode) and the reported mid-egress measurements errors, they may introduce systematics that affect orbital fits. Indeed, we find that the published data, when taken literally, cannot be explained by any unique solution. Many qualitatively different and best-fit 2-planet configurations, including self-consistent, Newtonian  $N$ -body solutions may be able to explain the data. However, using high resolution, precision OPTIMA light curves, we find that the (O-C) deviations are best explained by the presence of a single circumbinary companion orbiting at a distance of  $\sim 4.5$  AU with a small eccentricity and having  $\sim 7$  Jupiter-masses. This object could be the next circumbinary planet detected from the ground, similar to the announced companions around close binaries HW Vir, NN Ser, UZ For, DP Leo or SZ Her, and planets of this type around Kepler-16, Kepler-34 and Kepler-35.

**Key words:** extrasolar planets—LTT technique— $N$ -body problem—polar—star: HU Aqr

## 1 INTRODUCTION

Magnetic cataclysmic variables (CVs, polars, a.k.a. AM Her stars) are interacting close binary systems. They consist of a main sequence red dwarf secondary filling its Roche lobe, and a strongly magnetized white dwarf (WD) primary, with typical magnetic field values of 10–80 MG (Schwöpe et al. 2001). The strong magnetic field of the primary interacts with the weaker magnetic field of

the secondary and locks the two stars together. Hence, the synchronously rotating WD spins at the same rate as the orbital mean motion of the binary. Under the gravitational field of the primary, material flows from the donor star initially along the binary orbital plane, and finally is accreted quasi-radially onto the magnetic poles of the WD. The variable HU Aquarii system (hereafter HU Aqr) belongs to this class of CV binaries hosting a strongly magnetic WD accompanied by a red dwarf (spectral type M4V) with an orbital

period of about 125 minutes. This system is one of the brightest polars in the optical domain with visual magnitudes ranging from 14.6 to 18 (Warner 1995; Hellier 2001), as well as in the X-ray energy range. Therefore, it has also been one of the most studied systems so far.

Accreted matter leaving from the red dwarf is initially not affected by the magnetic field of the WD. The matter follows a ballistic trajectory up to the moment when the WD magnetic field begins to dominate. Because the WD magnetosphere extends beyond the  $L_1$  radius, the plasma stream cannot orbit freely, and thus does not form an accretion disk, unlike in other non-magnetic cataclysmic variables. The accreted matter follows the magnetic field lines and forms an accretion spot at the magnetic poles of the WD. In many systems, the WD magnetic field is tilted in a such way that one magnetic pole is oriented toward the direction of flowing matter. Eclipses observed in highly inclined polars provide information about the stream geometry.

According to the most recent work of Schwöpe et al. (2011) the inclination of the binary is  $\sim 87^\circ \pm 0.8^\circ$ . This special geometry is important for the planetary hypothesis investigated in this work. Assuming that a planetary companion (or companions) have formed in the circumbinary disc, the inclination constraint removes the mass indeterminacy inherent to the eclipse timing method.

Recently, the HU Aqr system has received much attention in the literature. Schwarz et al. (2009) carried out an analysis of the light curves of the system and derived mid-egress times of the polar. They proposed a planetary companion as one possible explanation of the detected (O-C) variability. Shortly after this work, Qian et al. (2011) presented and discussed 10 new light curves in the optical domain. These authors confirmed the deviations of the observed mid-egress times from a linear or quadratic ephemeris, concluding that the large (O-C) residuals may be explained by the Light Travel Time [LTT aka Roemer effect, Irwin (1952)] due to two jovian-mass planetary companions in orbits with semi-major axes of a few AU and a moderate eccentricity of  $\sim 0.5$  for the outer planet. The orbit of the inner planet was fixed to be circular. The ratio of the orbital periods of these massive putative planets would be presumably in a low-order 2c:1b mean motion resonance (MMR). The latter points to significant mutual interactions between these objects which strongly affects the orbital stability of the system. Indeed, shortly after that work was published, Horner et al. (2011) performed dynamical analysis of the putative HU Aqr 2-planet system, exploring the parameter space within  $3\sigma$  uncertainty levels of the derived Keplerian elements. They found that none of the best-fit configurations presented by Qian et al. (2011) were dynamically stable implying that the planetary hypothesis proposed by these authors is hard to maintain. After a few months, in a new paper, Wittenmyer et al. (2012) also re-analysed data in Qian et al. (2011) confirming that the 2-planet configuration is mathematically consistent with the observations, but inferred orbits are catastrophically unstable over a  $\sim 10^3$ – $10^4$  year time-scale. Furthermore, in a very recent paper, Hinse et al. (2012) improved the Keplerian fit models of this system by imposing orbital stability constraints on the objective function  $(\chi^2_{\nu})^{1/2}$ . Although these authors were able to find a *stable* 2-planet configuration consistent with the linear ephemeris model, orbital parameters of these planets were relatively distant from the formal best-fit solution by more than  $3\sigma$ . Because the results of extensive dynamical analysis contradict the 2-planet hypothesis, an alternative explanation of the (O-C) diagrams needs to be considered.

Long term monitoring of HU Aqr shows large variations of the accretion rate that could be correlated with a migration of the

accretion spot. Taking into account the observed changes of the accretion geometry during different accretion states, high and intermediate ones, Schwöpe et al. (2001) estimated the possible time-shift of eclipses to be on the level of 2 seconds, which is still much smaller than the deviations between the theoretical ephemeris and observed mid-egress moments. These results suggest that the migration of the accretion spot cannot be responsible for the (O-C) deviations, and we therefore ruled it out.

The (O-C) variability of HU Aqr could be also attributed to other complex astrophysical phenomena in the binary, like the Applegate mechanism and/or magnetic braking discussed by Schwarz et al. (2009) and Wittenmyer et al. (2012). The timing signal might also be affected by non-Gaussian red-noise, which is a well known effect present in the precision photometry of transiting planets and timing of millisecond pulsars (e.g., Pont et al. 2006; Coles et al. 2011). Hence, it should be stressed that we focus here on the planetary hypothesis, as one of the possible, simple and somehow attractive explanations of the (O-C) variability. We try to solve “the puzzle” of unstable 2-planet models through a new and independent analysis of available data, conducted along three basic directions.

The first one relies on the re-analysis of published data, because we found a few inconsistencies in the literature. Surprisingly, while in the recent paper, Wittenmyer et al. (2012) take into account 82 mid-egress points from Schwarz et al. (2009) and Qian et al. (2011), this is not the full data set available in the literature at that time. In fact, 72 egress times published by Schwarz et al. (2009) extend the data set in Schwöpe et al. (2001) that included 31 measurements. Although the early data of Schwöpe et al. (2001) spanning cycles 0–22478 overlap with measurements in Schwarz et al. (2009) in the time window covering cycles 1319–60097, they may be helpful to constrain the best-fit models. Up to now, the full list of published observations consists of 113 points, including data in Qian et al. (2011). Yet it is not quite obvious whether Qian et al. (2011) included measurements in Schwöpe et al. (2001) in their analysis. Hinse et al. (2012) considered the full data set available at that time, but in terms of the linear ephemeris LTT model only. In this context, a direct comparison of the results in the published papers is difficult.

The second aspect of our study is a new kinematic model of the ephemeris that properly approximates orbits of putative companions in multi-body systems (to the lowest possible order in the masses), as compared to the full  $N$ -body model. The kinematic model used in all cited papers refers back to Keplerian parametrization by Irwin (1952) for the “one companion” case. That model, though commonly used in the literature (e.g., Lee et al. 2011), seems nowadays redundant, as it was introduced to quantify a similarity between the LTT and the radial velocity curves, in a particular reference frame with the origin at the center of the two-body LTT orbit (instead of the dynamical barycenter). Indeed, the recent, although short history of modeling precision radial velocities teaches us that multiple planetary systems should be modeled either using kinematic formulation in a proper coordinate frame (e.g. Lee & Peale 2003; Goździewski et al. 2003), or using the most general and accurate full  $N$ -body model (Laughlin & Chambers 2001). The dynamical stability can be further incorporated as an additional, *implicit* observable to the objective function (e.g., Goździewski & Maciejewski 2001; Goździewski et al. 2008). In this work we are focused on the kinematic modeling though the self-consistent  $N$ -body approach was also used to analyse the HU Aqr mid-egress times (see Appendix). Our results indicate that the Newtonian model may be required for other systems presumably exhibiting the LTT effect, indeed.

The third and, actually, critical direction of our work, is a careful independent analysis of the significantly extended data set including already published egress times, and new high-precision timing of the egresses obtained with the ultra-fast photometer OPTIMA (Kanbach et al. 2003, 2008), as well as the MONET/N, PIRATE and TCS telescopes. We collected almost 60 new egress times with superior accuracy at the sub-second level. Moreover, we found that the literature data are non-homogeneous, as they come from different instruments with different time resolutions, as well as working in different spectral windows (from the visual range, through the UV, to the X-ray domain) and non/polarimetric modes. Taking into account the above mentioned inhomogeneities factors and new data, we present the results from a quasi-global optimization of two basic LTT models, leading us to the conclusion that the measured (O-C) data of HU Aqr may be best explained by a 1-planet configuration. Simultaneously, it would resolve the 2-companions instability paradox in the simplest way.

This paper is structured as follows. In Sect. 2 we derive 2-planet LTT models on the basis of Jacobi coordinates which describes kinematic orbits in multiple systems properly, as well as a hybrid optimisation algorithm and numerical setup that makes it possible to explore the  $(\chi^2_{\nu})^{1/2}$  parameter space in a quasi-global manner. We also briefly describe the  $N$ -body formulation of the LTT effect. In Sect. 3, we re-analyse the data set published in the literature, following the 2-planet hypothesis by Qian et al. (2011) and further investigated by Wittenmyer et al. (2012). Two examples of highly degenerate best-fit solutions are found. In Sect. 4, possible effects of different spectral windows for the light curves and determination of egress times are studied. Furthermore, we describe the new data set derived with the OPTIMA and other instruments. In Sect. 5, we propose the 1-planet model that best explains the (O-C) variability. We briefly discuss the effect of red-noise in Sect. 6 and present a summary of our work in the Conclusions, Sect. 7. The Appendix contains extensive supplementary material to Sect. 5, including the results of kinematic and  $N$ -body modeling of 2-planet systems, accompanied by the long-term stability tests.

## 2 LTT MODEL FOR A 2-PLANET SYSTEM

We briefly develop the Keplerian model of the LTT signal in the three-body configuration, assuming that a compact binary (like HU Aqr) has *two* planetary companions. More technical details and a generalization of that model will be published elsewhere (Goździewski et al., in preparation). We consider the compact binary as a *single* object having the mass of  $m_*$ , which is reasonable in accordance with the extremely short orbital period ( $\sim 125$  min) of the polar. A single companion, as well as multiple-planet models are particular cases of this problem. The key point is that the Keplerian (or *kinematic*) model requires special coordinates in order to preserve the sense of Keplerian elements as an approximation of the *exact*  $N$ -body initial condition. That can be accomplished by expressing the dynamics through particular canonical coordinates in which the mutual planetary interactions are possibly small with respect to the main, “pure” Keplerian part. The barycentric formulation (Irwin 1952) in fact ignores the interactions which could be adequate for low-mass circumbinary objects, but it might fail when they have stellar masses as in the SZ Her system (Lee et al. 2011) where companions are as massive as 20% of  $M_{\odot}$ , and can shift the system barycenter significantly. The reason for introducing this improved model is in fact the same as in the precision radial velocities analyses (e.g., Lee & Peale 2003; Goździewski et al. 2003).

### 2.1 Kinematic parametrization of the LTT effect

One of the well known frames that provides a proper description of kinematic orbits in multiple systems is Jacobi coordinates. Let us assume that  $m_*$ ,  $m_1$  and  $m_2$  represent the masses of the compact binary  $m_*$  and two planets, respectively. Let us also assume that the Cartesian coordinates of these objects with respect to the three-body barycentre are  $\mathbf{R}_*$ ,  $\mathbf{R}_1$ ,  $\mathbf{R}_2$ , and their Jacobi coordinates are denoted by  $\mathbf{r}_* \equiv \mathbf{R}_*$ ,  $\mathbf{r}_1$ ,  $\mathbf{r}_2$  (see Fig. 1). Here  $\mathbf{R}_*$  is the position of the centre of mass of the binary (CMB) in the barycentric frame, and  $\mathbf{r}_1$ ,  $\mathbf{r}_2$  are position vectors of the planetary companions in the Jacobi frame. In this formalism, the barycentric position of the binary is:

$$\mathbf{R}_* = -\kappa_1 \mathbf{r}_1 - \kappa_2 \mathbf{r}_2, \quad (1)$$

where the mass factor coefficients  $\kappa_1 \geq 0$ ,  $\kappa_2 \geq 0$  are given by:

$$\kappa_1 = \frac{m_1}{m_1 + m_*}, \quad \kappa_2 = \frac{m_2}{m_1 + m_2 + m_*}. \quad (2)$$

The coordinate transformation  $\mathbf{R} \rightarrow \mathbf{r}$  is taken from Malhotra (1993):

$$\begin{aligned} \mathbf{r}_* &\equiv \mathbf{R}_*, \\ \mathbf{r}_1 &= \mathbf{R}_1 - \mathbf{R}_*, \\ \mathbf{r}_2 &= \mathbf{R}_2 - \frac{m_* \mathbf{R}_* + m_1 \mathbf{R}_1}{m_1 + m_*}, \end{aligned} \quad (3)$$

and the inverse transformation is derived from the integral of the barycentre:

$$\begin{aligned} \mathbf{R}_* &= -\kappa_1 \mathbf{r}_1 - \kappa_2 \mathbf{r}_2, \\ \mathbf{R}_1 &= (1 - \kappa_1) \mathbf{r}_1 - \kappa_2 \mathbf{r}_2, \\ \mathbf{R}_2 &= (1 - \kappa_2) \mathbf{r}_2. \end{aligned} \quad (4)$$

To the first order in the mass-ratio ( $\sim m_{1,2}/m_*$ ), the true  $N$ -body orbit of body  $i$ , ( $i = 1, 2$ ) is described through geometric Keplerian elements as follows:

$$\mathbf{r}_i(t) = \mathbf{P}_i [\cos E_i(t) - e_i] + \mathbf{Q}_i \sqrt{1 - e_i^2} \sin E_i(t),$$

where

$$\mathbf{P}_i = a_i (\mathbf{l}_i \cos \omega_i + \mathbf{k}_i \sin \omega_i), \quad \mathbf{Q}_i = a_i (-\mathbf{l}_i \sin \omega_i + \mathbf{k}_i \cos \omega_i),$$

and geometric elements are defined through:

$$\mathbf{l}_i = \begin{bmatrix} + \sin \Omega_i \\ + \cos \Omega_i \\ 0 \end{bmatrix}, \quad \mathbf{k}_i = \begin{bmatrix} + \cos i_i \cos \Omega_i \\ - \cos i_i \sin \Omega_i \\ \sin i_i \end{bmatrix}.$$

Here,  $E_i(t)$  is the eccentric anomaly derived from the Kepler equation

$$n_i(t - T_i) = E_i(t) - e_i \sin E_i(t),$$

where  $n_i = 2\pi/P_i$  is the mean motion, in accordance with Kepler 3rd law,  $n_i^2 a_i^3 = \mu_i$ , where  $P_i$  is the orbital period of a given object. Two tuples  $(a_i, e_i, i_i, \Omega_i, \omega_i, T_i)$ ,  $i = 1, 2$ , that consist of the semi-major axis, eccentricity, inclination, nodal angle, argument of pericentre, and the time of pericentre passage, respectively, are for the geometric Keplerian elements. These are related to the Cartesian coordinates in the Jacobi frame through the usual two-body formulae (see, e.g. Morbidelli 2002), with an appropriate mass parameter  $\mu_i$  (see below).

From Eq. 1, the  $Z_*$  component of the CMB with respect to the system barycentre is:

$$Z_*(t) \equiv \mathbf{R}_* \cdot \mathbf{e}_z = -\kappa_1 z_1(t) - \kappa_2 z_2(t), \quad (5)$$

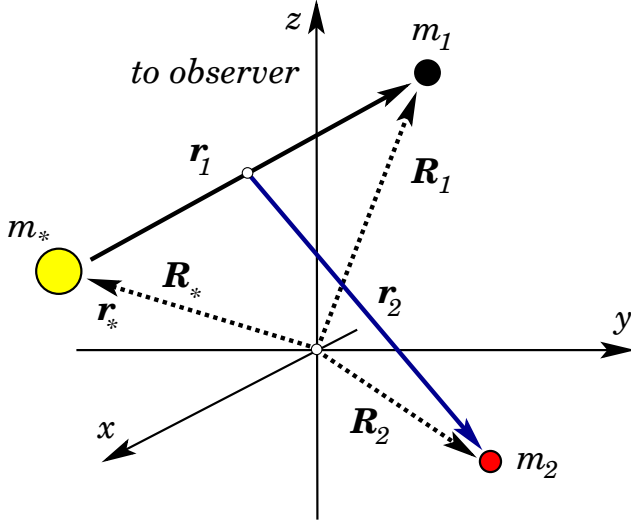


**Figure 1.** The geometry of the system. The binary has a total mass  $m_*$  and because of its short orbital period it can be considered as a point-like object accompanied by planets as point-masses. The origin of the coordinate system is fixed at the barycentre of the three-body system. The line-of-sight is along the  $z$ -axis. See the text for more details.

where  $\mathbf{e}_z$  is the unit vector along the  $z$ -axis of the reference frame, directed toward the observer. The signal contribution due to a given companion is:

$$z_i(t) = a_i \sin i_i \left[ \sin \omega_i (\cos E_i(t) - e_i) + \cos \omega_i \sqrt{1 - e_i^2} \sin E_i(t) \right] \quad (6)$$

(for planets  $i = 1, 2$ ). The  $z_i(t)$  are then combined to obtain the  $Z_*(t)$  component of the CMB position vector w.r.t. the system barycentre. The LTT signal is then expressed as:

$$\tau(t) = -\frac{1}{c} Z_* \equiv +\frac{1}{c} \left( \frac{m_1}{m_1 + m_*} z_1 + \frac{m_2}{m_1 + m_2 + m_*} z_2 \right),$$

where  $c$  is the speed of light. Note that we used the planetary version of the three-body system, with *one* dominant mass ( $m_*$ ), hence the gravitational Keplerian parameters are:

$$\mu_1 = k^2(m_1 + m_*), \quad \mu_2 = k^2 \frac{m_*(m_1 + m_2 + m_*)}{m_1 + m_*},$$

consistent with the expansion of the Hamiltonian perturbation for the planetary version of the problem (see, e.g., Malhotra 1993), and the quantity  $k$  denotes the Gauss constant.

We introduce the signal semi-amplitude factors,  $K_1$  and  $K_2$  as:

$$K_1 = \left( \frac{1}{c} \right) \frac{m_1}{m_1 + m_*} a_1 \sin i_1, \quad (7)$$

$$K_2 = \left( \frac{1}{c} \right) \frac{m_2}{m_1 + m_2 + m_*} a_2 \sin i_2. \quad (8)$$

Using Eq. 6, the single-planet signal contributions  $\zeta_i$  are then given by:

$$\zeta_i(t) = K_i \left[ \sin \omega_i (\cos E_i(t) - e_i) + \cos \omega_i \sqrt{1 - e_i^2} \sin E_i(t) \right]. \quad (9)$$

In this equation, the set of free orbital parameters is  $(K_i, P_i, e_i, \omega_i, T_i)$ ,  $i = 1, 2$ , similar to the common kinematic radial velocity model. The orbital period  $P_i$  and the time of pericenter passage are introduced indirectly through the time dependence expressed by  $E_i(t)$ .

We would like to note here that the contribution of the planet as expressed in Irwin’s model has an extra term  $e_i \sin \omega_i$  that appears due to the particular choice of the coordinate system with the origin at the center of the binary orbit around the common center of mass of the system. It should also be stressed, that no simple superposition of kinematic orbits does account for the mutual gravitational interactions directly, but in our formulation, the Keplerian elements are the closest to the osculating  $N$ -body initial condition within the kinematic model.

## 2.2 The (O-C) formulation

From Eq. 9, the fit model of the planetary-induced LTT signal is

$$\tau(t, K_1, P_1, e_1, \omega_1, T_1, K_2, P_2, e_2, \omega_2, T_2) = \zeta_1(t) + \zeta_2(t).$$

Now let us assume that the observational data are given through eclipse cycle number  $l$  ( $l = 0, \dots, N$ ), the date of the eclipse time-mark  $t_l$ , and its uncertainty  $\sigma_l$ . Then the  $l$ -cycle eclipse ephemeris with respect to the reference epoch  $t_0$  ( $l = 0$ ), at time  $t \equiv t_l$  may be written as follows:

$$T_{\text{ep}}(l) = t_0 + lP_{\text{bin}} + \tau(t_l, K_{1,2}, P_{1,2}, e_{1,2}, \omega_{1,2}, T_{1,2}) + \text{“physics”},$$

where  $P_{\text{bin}}$  is the orbital period of the binary. It should not be assumed as known in advance, hence must be fitted, as well as the initial epoch  $t_0$  corresponding to cycle number  $l = 0$ , simultaneously with other parameters of the model. The term coded as “physics” contains *non-Keplerian* effects, such as the period damping or other phenomena that may/should be included in the fit model. Here, we introduce two instances of such a model. Following Hilditch (2001), the *linear ephemeris* model, as above,

$$(\text{O-C}) = T_{\text{ep}}(l) - t_0 - lP_{\text{bin}} = \tau(t_l, K_{1,2}, P_{1,2}, e_{1,2}, \omega_{1,2}, T_{1,2}), \quad (10)$$

and the *quadratic ephemeris* model, the simplest, yet non-trivial generalization of the polynomial ephemeris (Hilditch 2001)

$$(\text{O-C}) = T_{\text{ep}}(l) - t_0 - lP_{\text{bin}} - \beta l^2 = \tau(t_l, K_{1,2}, P_{1,2}, e_{1,2}, \omega_{1,2}, T_{1,2}). \quad (11)$$

The quantity  $\beta$  in Eq. 11 is a factor that describes the binary period damping (change) due to the mass-transfer, magnetic braking, gravitational radiation, and/or influence of a very distant companion

$$\beta = \frac{1}{2} P_{\text{bin}} \dot{P}_{\text{bin}}.$$

Let us note that also  $\beta$  should be fitted simultaneously with other free parameters of the model. In the rest of this paper, we use a common notation in the extrasolar planets literature, that enumerates the planets by subsequent letters, i.e., “b”  $\equiv$  “1”, “c”  $\equiv$  “2”, etc., to avoid any confusion.

## 2.3 Newtonian model of the LTT effect

A derivation of the  $N$ -body model of the LTT is basically very simple. It requires the computation of the planetary contribution  $\tau$  to the (O-C) signal through the numerical integration of the equations of motion, a computation of the star barycentric vector  $\mathbf{R}_*$  and its  $Z_*$ -component, in accord with Eq. 5. This formulation accounts for the mutual interactions between all bodies in the system. A serious computational drawback of this model is a significant CPU overhead, nevertheless, as we will show in the Appendix, its application for systems with massive companions presumably involved in low order mean motion resonances can be indispensable. To solve the equations of motion efficiently, we used the ODEX2

integrator (Hairer et al. 2009) designed for conservative, second order ordinary differential equations (ODEs). The imposed variable time step accuracy preserved the total energy and the angular momentum better than  $10^{-11}$ . In terms of the Newtonian model, the planetary bodies are parametrised through the mass  $m_i$ , semi-major axis  $a_i$ , eccentricity  $e_i$  and three Keplerian angles describing the orientation of the orbit, for each companion in the system. We also assume that the binary is a point mass with the prescribed total mass of the binary. Assuming a coplanar configuration (in the  $N$ -body model the same inclinations are “absorbed” in the planetary masses), we have 5 free orbital parameters for each planet, similar to the kinematic model. Here, they are then represented as “usual” osculating, astrometric Keplerian elements at a given initial epoch, but other types of the osculating elements may be used as well.

#### 2.4 The optimization method and numerical setup

Having the egress times measured with a great precision (at the 1 second level, or even better), the next step is to determine the set of primary parameters of the kinematic model, usually with the least squares approach, by constructing the reduced  $(\chi_v^2)^{1/2}$ -squared function

$$(\chi_v^2)^{1/2} \equiv (\chi_v^2)^{1/2}(K_{1,2}, P_{1,2}, e_{1,2}, \omega_{1,2}, T_{1,2}, t_0, P_{\text{bin}}, \beta),$$

and searching for its minimum in the space of the model parameters. It is well known, however, that the  $(\chi_v^2)^{1/2}$  function may possess many local minima, particularly if the model is not well constrained, as it might be in our case. To seek a global solution, we apply a hybrid algorithm that consists of two steps: a quasi-global method, the Genetic Algorithm [GA, Charbonneau (1995)] that is relatively slow and inaccurate, but makes it possible to find good approximations to the second step, a fast local method. Here, we use the Levenberg-Marquardt (L-M) algorithm with analytically computed derivatives. The idea of the hybrid code comes from our earlier works on modelling radial velocity observations (e.g., Goździewski & Konacki 2004). We used freely available Fortran codes of the Genetic Algorithm (PIKAIA<sup>1</sup>, by Phil Charbonneau & Barry Knapp) and of the L-M method from the well known MINPACK<sup>2</sup> package.

Once the primary set of the orbital model parameters are determined in the form of two five-tuples  $(K_i, P_i, e_i, \omega_i, T_i)$ ,  $i = 1, 2$ , we may also derive inferred Keplerian elements, such as *minimal* planetary masses and semi-major axes, by solving nonlinear equations expressing  $K_i$  (Eqs. 7, 8) and the 3rd Kepler law in terms of the primary model parameters. The inclination has to be held fixed. Hence usually one assumes  $i_i = 90^\circ$ . Let us underline that while the LTT-model (Eq. 9) formulated in the barycenter frame has the same mathematical form as in the Jacobi frame, the orbital, geometrical (Keplerian) elements in multiple systems should be related to Jacobian, canonical coordinates. If in the  $N$ -body numerical integrations and stability studies, initial conditions have to be in the form of osculating elements, one should transform these Jacobian elements into the Cartesian coordinates w.r.t. the Jacobi frame (e.g., Morbidelli 2002), and then, if necessary, to the astrometric or barycentric coordinates. In this sense, “barycentric” and “Jacobian” two-body elements may closely coincide for small, Jovian-mass planets. But for more massive companions when the LTT signal is easier to detect, or for very compact (resonant) systems, the semi-major

axes, masses, Keplerian angles and inferred  $N$ -body initial conditions may be significantly different in both frames. We will discuss this issue in more detail in a forthcoming article (Goździewski et al., in preparation).

Each run of the hybrid code has been initiated by random selection of the GA population (between 512 and 4096 individuals), considering possibly wide parameter ranges. For instance, the range of orbital periods was set blindly to [800, 63600] days, and angles and eccentricities were set to their whole possible ranges. The original “population” was then transformed by GA operators over 512–1024 generations. Each member of the final set was then used as an initial condition for the L-M algorithm, and the resulting solutions were sorted and stored. The hybrid procedure was repeated hundreds of times for each combination of model–data set. We examined whether the obtained solutions converged to the same minima. Due to the semi-deterministic nature of the GAs, one should interpret the results in a statistical sense.

The same procedure may be applied to the Newtonian model, as the planetary contribution  $\tau$  can be computed independently of the optimisation method. (In this case the derivatives to the LM algorithm were approximated numerically).

Finally, uncertainties of the best-fit parameters were determined using the bootstrap algorithm (Press 2002), as the variances of parameters in a tested solution that has been re-fitted to 4096 synthetic data sets drawn randomly with replacement from the original sample. We found that due to the particular distribution of OPTIMA observations that are grouped in small “clumps” of a few data points, the bootstrap algorithm tends to underestimate the uncertainties when compared to the formal error determination through the diagonal elements of  $(\chi_v^2)^{1/2}$  curvature (covariance) matrix.

### 3 KINEMATIC MODELING THE LITERATURE DATA

To verify the literature models of the HU Aqr system, we gathered Barycentric Julian Dated (BJD) egress times published by Schwöpe et al. (2001), Schwarz et al. (2009) and Qian et al. (2011). That data set consists of 113 points, and will be called the SSQ set hereafter. Our first attempt was to reproduce the results of Qian et al. (2011) with our formulation of the LTT model. We did not expect this to be straightforward, since their model assumes the inner planet to be on a circular orbit. We conducted calculations for two ephemeris models, linear and quadratic (Eqs. 10 and 11), respectively.

#### 3.1 The linear kinematic ephemeris 2-planet model

In the linear ephemeris case, we found many, almost equally good 2-planet solutions with  $(\chi_v^2)^{1/2} \sim 1.15$  and an rms  $\sim 2.3$  sec. In these best fits the inner planet has a period of  $\sim 5500 - 6000$  days. However, the period of the outer planet varies between 7000–20000 days. The resulting systems imply (O-C) residuals caused individually by the planets in wide ranges, up to  $\sim 6000$  seconds, and companions in basically any mass, eccentricity and period range while still preserving excellent rms  $\sim 2.3$  sec and similar “flat” behaviour of the residuals. The left panel of Fig. 2 shows the most exotic and actually the best-fit solution found in our experiment. The Keplerian fit parameters of this solution, as well as its inferred elements are given in Table 1 (Fit A). This fit is very different from those found by Qian et al. (2011), Wittenmyer et al. (2012), and even in the last paper by Hinse et al. (2012). This configuration has  $(\chi_v^2)^{1/2} \sim 1.143$  and an rms  $\sim 2.3$  sec, and is characterised by

<sup>1</sup> <http://www.hao.ucar.edu/modeling/pikaia/pikaia.php>

<sup>2</sup> <http://www.netlib.org/minpack/>

almost equal orbital periods of  $\sim 5470$  days. The pericenter arguments of the planets in this fit differ by nominal value of  $180.2^\circ$  and as a result, the Keplerian barycentric orbits are almost exactly anti-aligned, with planets placed close to their periastrons at the initial epoch. This configuration could be understood as a pair of *Trojan-planets* in 1c:1b mean motion resonance (MMR). Although the resulting LTT signal has apparently small amplitude  $\sim 60$  seconds as shown in the (O-C) diagram (see the left-hand panel in Fig. 2), the LTT semi-amplitudes  $K_{b,c}$  are excessively large (up to  $\sim 6000$  seconds), implying just absurdly massive companions of  $\sim 10,000$  Jupiter mass each ( $\sim 10 M_\odot$ !). This solution reveals that an inherent degeneracy of the LTT signal (and its model) may appear because the signal is the result of the *differential* gravitational tugs of the companions on the binary. Indeed, in this particular Trojan configuration, even small deviations from the anti-alignment of orbits leads to large changes in the planetary masses (over 3 orders of magnitude) and semi-major axes (within a range of a few AU), indicating that as they are not supported by the currently available observations, these dynamical parameters are poorly constrained. The mathematical fit permits putative companions as massive as stars but in reality, such objects should influence dynamical and spectral properties of the binary system. Such solutions are therefore excluded.

The 1c:1b MMR solution is a vivid example demonstrating that due to the possibility of configurations involved in extremely strong mutual interactions, modeling the LTT signal globally (without any *a priori* assumptions on the system configuration) cannot be studied in terms of the kinematic model. In general, an exact, self-consistent  $N$ -body model should be used to determine the initial conditions.

### 3.2 The quadratic kinematic ephemeris 2-planet model

In the case of a quadratic ephemeris, we found a well defined minimum of  $(\chi^2_{\nu})^{1/2} \sim 0.972$ , which is an apparently statistically perfect solution. Its synthetic curve with measurements over-plotted is shown in the right-hand panel of Fig. 2, and orbital parameters are given in Table 1 as Fit B. That solution has been frequently found in different runs of the hybrid code, which reinforces its global character. To show the latter, we computed parameter scans of  $(\chi^2_{\nu})^{1/2}$  in the  $(P_{b,c}, e_{b,c})$ -planes (Fig. 3), by fixing points of a grid in a given plane and minimizing  $(\chi^2_{\nu})^{1/2}$  over all remaining free parameters of the model. This made it possible to obtain standard confidence levels as marked with coloured curves. The best-fit solution is again very different from solutions found in the literature. While the elements of the inner planet are well constrained, the orbit of the outermost companion reveals extremely large eccentricity ( $\sim 1$ ). That points again to highly degenerate (unrealistic) best-fit solutions, with near-parabolic or even hyperbolic, open orbit of one “planet” — as the fit implies — being a low-mass stellar object of  $\sim 160$  Jupiter-masses. Other solutions with slightly worse  $(\chi^2_{\nu})^{1/2} \sim 1.1$  and still very similar rms  $\sim 2.2$  sec may be found too, which means that the quadratic ephemeris model is unconstrained by the SSQ data.

In the quadratic ephemeris model, the orbital periods are close to the 4:3 ratio, which is equivalent to the low-order 4c:3b mean motion resonance. In addition, the eccentricity of the outer planet is extreme, close to 1. Hence again, the kinematic formulation seems inadequate to derive the proper initial condition of the multiple-planet configuration. We conclude here that when we only have the SSQ data at our disposal, there seems to be no unique and phys-

**Table 1.** Jacobian geometric parameters with the inferred masses and semi-major axes of 2-planet LTT fit models *in the barycenter frame* with the linear and parabolic ephemeris to the SSQ data set. Synthetic curves with data sets are shown in two panels of Fig. 2 and  $(\chi^2_{\nu})^{1/2}$  scans in Fig. 3. Numbers in parentheses represent the uncertainties at the last significant digit. Total mass of the binary is  $1.08 M_\odot$  (Schwarz et al. 2009). Indices “b” and “c” refer here to planets “1” and “2” in the mathematical model Eqs. 10 and 11. See the text for more details.

Model parameter	Fit A linear ephemeris	Fit B parabolic ephemeris
$K_b$ [seconds]	$5928 \pm 15$	$10.2 \pm 0.5$
$P_b$ [days]	$5467 \pm 418$	$2910 \pm 28$
$e_b$	$0.138 \pm 0.034$	$0.34 \pm 0.07$
$\omega_b$ [degrees]	$207 \pm 21$	$22 \pm 8$
$T_b$ [BJD 2,440,000+]	$11694 \pm 175$	$5652 \pm 97$
$K_c$ [seconds]	$5942 \pm 17$	$322 \pm 30$
$P_c$ [days]	$5476 \pm 424$	$3931 \pm 50$
$e_c$	$0.141 \pm 0.035$	$0.99 \pm 0.05$
$\omega_c$ [degrees]	$27 \pm 20$	$358.3 \pm 0.2$
$T_c$ [BJD 2,440,000+]	$6214 \pm 451$	$9207 \pm 42$
$P_{\text{bin}}$ [days]	0.086820400(4)	0.0868204250(8)
$T_0$ [BJD 2,440,000+]	9102.92004(2)	9102.91988(2)
$\beta$ [ $\times 10^{-13}$ day cycle $^{-2}$ ]	—	-3.06(6)
$a_b$ [au]	1.375	4.08
$m_b \sin i$ [ $M_{\text{Jup}}$ ]	9780	5.69
$a_c$ [au]	1.374	4.58
$m_c \sin i$ [ $M_{\text{Jup}}$ ]	9811	159
$N$	113	113
$(\chi^2_{\nu})^{1/2}$	1.143	0.972
rms [seconds]	2.31	2.13

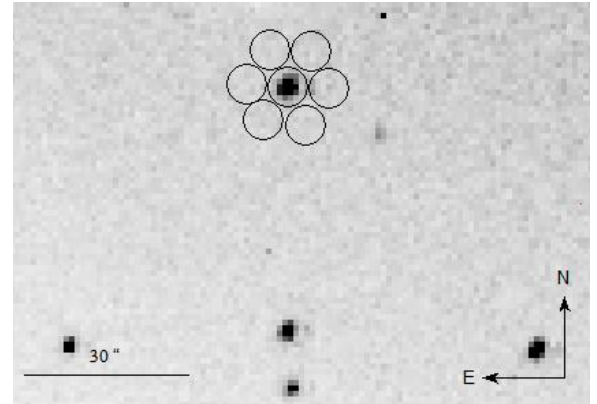


**Figure 4.** OPTIMA hexagonal fibre bundle centred on HU Aqr. The ring fibres (1–6) are used to monitor the background sky simultaneously.

ically meaningful solution explaining the LTT variability. Or, the planetary fit model and its assumptions are incorrect.

## 4 NEW OBSERVATIONS AND DATA REDUCTION

### 4.1 Observations with OPTIMA and other instruments

To resolve the model degeneracies as described above, we gathered new, yet unpublished observations of the HU Aqr binary. The new collected mid-egress BJD times are given in Table 2. These data ex-

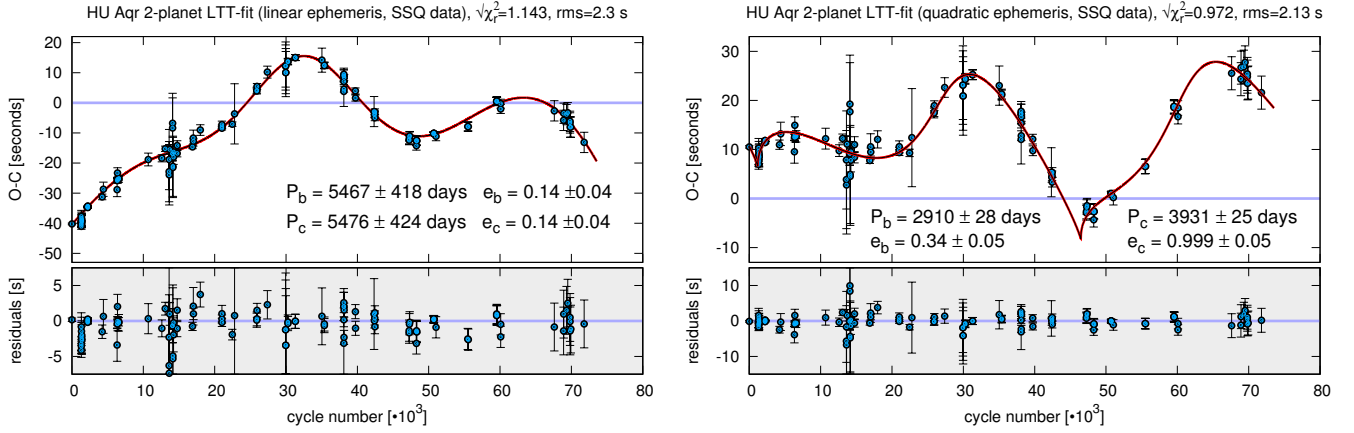


**Figure 2.** Synthetic curves of the best-fit, 2-planet solutions to the mid-egress BJD times of the SSQ data set. The left panel corresponds to a linear ephemeris model (Eq. 10) and the right panel corresponds to a quadratic (parabolic) ephemeris model (Eq. 11, the parabolic trend has been removed). Panels are labeled with the orbital periods and eccentricities of the putative companions. Bottom plots with shaded background show the residuals after subtracting planetary and astrophysical contributions from the LTT signal. Discontinuous-like features of the parabolic ephemeris model around cycles 0 and 46,000 appear due to the extreme eccentricity of the outer body. See Table 1 for the orbital and inferred elements (Fit A and B, respectively).

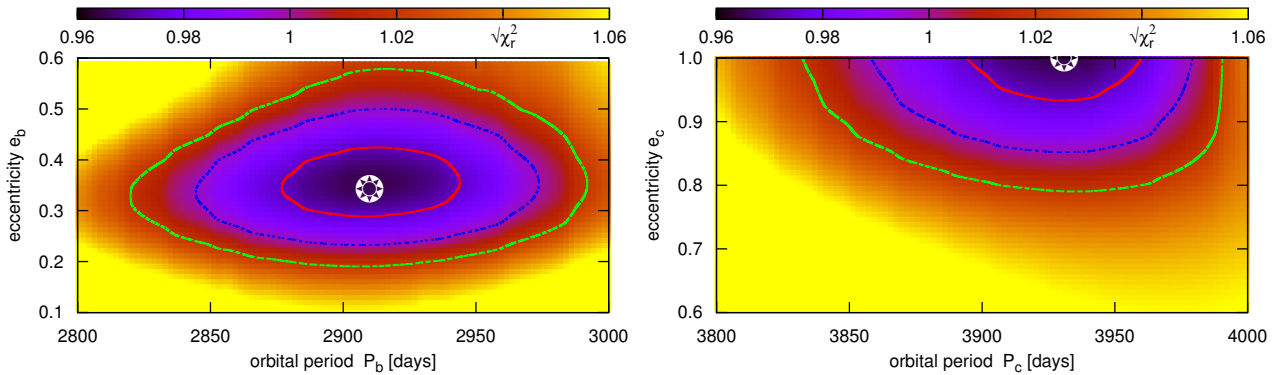


**Figure 3.** Parameter scans of the  $(\chi_v^2)^{1/2}$  function computed around the best fit solution to the SSQ data for the quadratic ephemeris model (see the right-hand panel in Fig. 2 and Fit B in Table 1). Colour curves are for the formal 1,2,3 $\sigma$ -levels of the best-fit solution whose parameters are marked with an asterisk.

tend the work of Schwöpe et al. (2001), Schwarz et al. (2009) and Qian et al. (2011). The currently available data set of HU Aqr egress times consists of 171 measurements in total, including 10 points presented in Qian et al. (2011). Among these measurements, 68 were obtained with the Optical Timing Analyzer (OPTIMA) instrument that operates mostly at the 1.3 m telescope at Skinakas Observatory, Crete, Greece.

The high-speed photometer OPTIMA is a sensitive, portable detector to observe extremely faint optical pulsars and other highly variable astrophysical sources. The detector contains eight fibre-fed single photon counters — avalanche photodiodes (APDs), and a GPS for the time control. There are seven fibres in the bundle (Fig. 4) and one separate fibre located at a distance of  $\sim 1'$ . Single photons are recorded simultaneously and separately in all channels with absolute UTC time-scale tagging accuracy of  $\sim 4 \mu\text{s}$ . The quantum efficiency of the APDs reaches a maximum of 60% at 750 nm and lies above 20% in the range 450–950 nm (Kanbach et al. 2003, 2008). During the HU Aqr observations, OPTIMA was pointed at RA(J2000) =  $21^{\text{h}}07^{\text{m}}58^{\text{s}}.19$ , Dec(J2000) =  $-05^{\circ}17'40''.5$ , corresponding to the central aperture of the fibres bundle (Fig. 4). For sky background monitoring, we usually choose one out of the six hexagonally located fibres. We look for the fibre

that is not by chance pointed to any source, therefore records sky background, and its response is the most similar to the central fibre response when the instrument is targeted at the dark sky. An example of a sky background subtracted light curve is shown at the top left-hand panel in Fig. 5.

We derived new fits to the HU Aqr eclipse egress times, as well as reanalysed many of the already published OPTIMA data. There are 26 eclipses obtained by OPTIMA published by Schwarz et al. (2009). We were able to reanalyse only 21 out of the 26 light curves, because only those were available in the OPTIMA archive. Our completely new data set includes 42 precision photometric observations, starting from cycle  $l \sim 29,900$ , overlapping in time window with the literature data. We derived 23 new eclipse profiles from the OPTIMA data archive spanning 1999–2007 and obtained 19 new OPTIMA optical HU Aqr light curves in 2008–2010. Note that some of the OPTIMA observations have been already published in the very recent literature (Nasiroglu et al. 2010).

We also gathered and reduced 11 observations performed at the MONET (MONitoring NETwork of Telescopes) project which is a network of two 1.2 m telescopes operated by the Georg-August-Universität Göttingen, the McDonald Observatory, and the South African Astronomical Observatory. These precision data in white

light (500–800 nm) were binned in 5 s intervals, with  $10^{-6}$  days (0.1 s) accuracy, separated by 3 s readout. The most recent observations were performed at November 18th, 2011.

An additional three egress times were obtained from the eclipse observations carried out with the PIRATE telescope equipped with the SBIG STL1001E CCD camera (Holmes et al. 2011). PIRATE, funded by the Open University Department of Physics and Astronomy, is a remote-controlled telescope located at the Astronomical Observatory of Mallorca (OAM), Spain.

We also performed optical observations of HU Aqr in white light with the 1.5-m Carlos Sánchez Telescope (TCS) equipped with Wide FastCam (WFC, Fig. 6). The WFC is a  $1k \times 1k$  – pixel camera with optics offering a FOV of 12 arcmin with a scale of 0.6 arcsec/pix. HU Aqr eclipses were observed on September 30, and October 01, 2011 with integration times of 3 and 5 seconds, respectively. WFC works in frame transfer mode, therefore the readout time is effectively null or in other words is equivalent to the exposure time. UTC mid-exposure times of the photometric measurements were converted to the Barycentric Julian Dates in Barycentric Dynamical Time using the procedure developed by Eastman et al. (2010).

Some technical details of the observations performed with the MONET/N, TCS, and PIRATE telescopes are given in Table 3.

#### 4.2 Determining time markers of the eclipses

In Fig. 5 we show an example of HU Aqr high time resolution OPTIMA photometric (see the right top panel, and blue curve in the left-hand top panel) and polarimetric (Stokes I, red curve in the right-hand top panel) light curves. These graphs are to be compared with the light curves from TCS, obtained with 3 and 5 seconds exposures illustrated in Fig. 6. Obviously, the OPTIMA resolution makes it possible to track the egress phase closely, which enabled us to determine the mid-egress moments very precisely.

Measuring the time of mid-egress properly is critical to obtain the (O-C) diagrams, since it is the time marker of the eclipse (Schwope et al. 2001; Schwarz et al. 2009). To derive the mid-egress moment  $t_0$ , the sigmoid function

$$I(t) = a_1 + \frac{(a_2 - a_1)}{(1.0 + \exp([t_0 - t]/\Delta t))}, \quad (12)$$

parametrised by  $a_1, a_2$  and  $t_0$  was fitted to the light curve points in the egress phase of the eclipse, spanning preselected exponential scaling parameters  $\Delta t$ . We found that there is no strong dependence of the derived  $t_0$  on the adopted  $\Delta t$ . This can be seen in the bottom left-hand panel of Fig. 5 where three mid-egress times  $t_0$  are marked with black open squares. These moments are derived for three different choices of  $\Delta t$ : 0.1, 0.5 and 1.0, respectively. While these times depend on  $\Delta t$ , they fall within a 2 second range, as marked by a shaded strip at the bottom left-hand panel of Fig. 5. A half of that range ( $\sim 1$  second) may be typically estimated as the maximum possible error of  $t_0$  in the OPTIMA data set. The formal  $1\sigma$  uncertainty of the sigmoid fit in this case is still smaller and at the level of  $\sim 0.1$  second. Moreover, the shape of the eclipse may significantly depend on the spectral window. Panels in the right column of Fig. 5 illustrate the light curves of HU Aqr derived in the optical, white band domain (the blue curve) and in the polarimetric domain (Stokes I, the red curve). In the latter case, the egress looks quite different and spans over a longer time. Given that these two data sets were taken four years apart, the observed difference might have been caused by different emission states of the source.

**Table 2.** New HU Aqr BJD mid-egress times on the basis of light curves collected with: OPT-ESO22 — OPTIMA photometer installed at ESO (Chile), OPT-SKO — OPTIMA operated at the Skinakas Observatory (Crete), PIRATE — a telescope at the Astronomical Obs. of Mallorca, MONET/N — the network of telescopes at the McDonald Obs. and the SAO (South Africa), and WFC — the 1.5-m TCS (Canary Islands).

Cycle	BJD	Error [days]	Instrument
29946	2451702.8443352	0.0000037	OPT-ESO22
29957	2451703.7993545	0.0000038	OPT-ESO22
29958	2451703.8861705	0.0000034	OPT-ESO22
30265	2451730.5400324	0.0000041	OPT-SKO
30287	2451732.4500902	0.0000023	OPT-SKO
30299	2451733.4919357	0.0000033	OPT-SKO
30300	2451733.5787554	0.0000054	OPT-SKO
30310	2451734.4469740	0.0000031	OPT-SKO
30311	2451734.5337856	0.0000018	OPT-SKO
35469	2452182.3533852	0.0000030	OPT-SKO
38098	2452410.6041626	0.0000084	OPT-SKO
42486	2452791.5719484	0.0000015	OPT-SAO
42487	2452791.6587715	0.0000024	OPT-SAO
44534	2452969.3800760	0.0000033	OPT-NOT
44557	2452971.3769377	0.0000085	OPT-NOT
51020	2453532.4971595	0.0000100	OPT-SKO
51066	2453536.4909030	0.0000064	OPT-SKO
51067	2453536.5777278	0.0000033	OPT-SKO
55535	2453924.4913426	0.0000102	OPT-SKO
55627	2453932.4788164	0.0000061	OPT-SKO
55661	2453935.4307071	0.0000064	OPT-SKO
55719	2453940.4662754	0.0000162	OPT-SKO
60085	2454319.5242409	0.0000074	OPT-SKO
64657	2454716.4671496	0.0000053	OPT-SKO
64885	2454736.2622085	0.0000038	OPT-SKO
64886	2454736.3490181	0.0000016	OPT-SKO
65265	2454769.2539926	0.0000023	OPT-SKO
67791	2454988.5622710	0.0000029	OPT-SKO
67917	2454999.5016391	0.0000017	OPT-SKO
67918	2454999.5884526	0.0000054	OPT-SKO
68009	2455007.4891162	0.0000018	OPT-SKO
72099	2455362.5844371	0.0000032	OPT-SKO
72110	2455363.5394546	0.0000019	OPT-SKO
72121	2455364.4944885	0.0000029	OPT-SKO
72133	2455365.5363444	0.0000015	OPT-SKO
72225	2455373.5238044	0.0000048	OPT-SKO
72237	2455374.5656456	0.0000040	OPT-SKO
72248	2455375.5206715	0.0000040	OPT-SKO
72305	2455380.4694292	0.0000030	OPT-SKO
72351	2455384.4631748	0.0000024	OPT-SKO
72352	2455384.5499944	0.0000022	OPT-SKO
72421	2455390.5406108	0.0000013	OPT-SKO
73409	2455476.3190971	0.0000578	PIRATE
73559	2455489.3421698	0.0000578	PIRATE
73560	2455489.4290151	0.0001156	PIRATE
75467	2455654.9954277	0.0000040	MONET/N
75812	2455684.9484608	0.0000023	MONET/N
76721	2455763.8681410	0.0000035	MONET/N
77031	2455790.7824571	0.0000039	MONET/N
77066	2455793.8211556	0.0000077	MONET/N
77067	2455793.9079841	0.0000055	MONET/N
77078	2455794.8630179	0.0000065	MONET/N
77546	2455835.4949490	0.0000179	WFC
77557	2455836.4499905	0.0000295	WFC
77789	2455856.5922852	0.0000038	MONET/N
77802	2455857.7209399	0.0000090	MONET/N
77823	2455859.5441786	0.0000066	MONET/N
78100	2455883.5934038	0.0000022	MONET/N

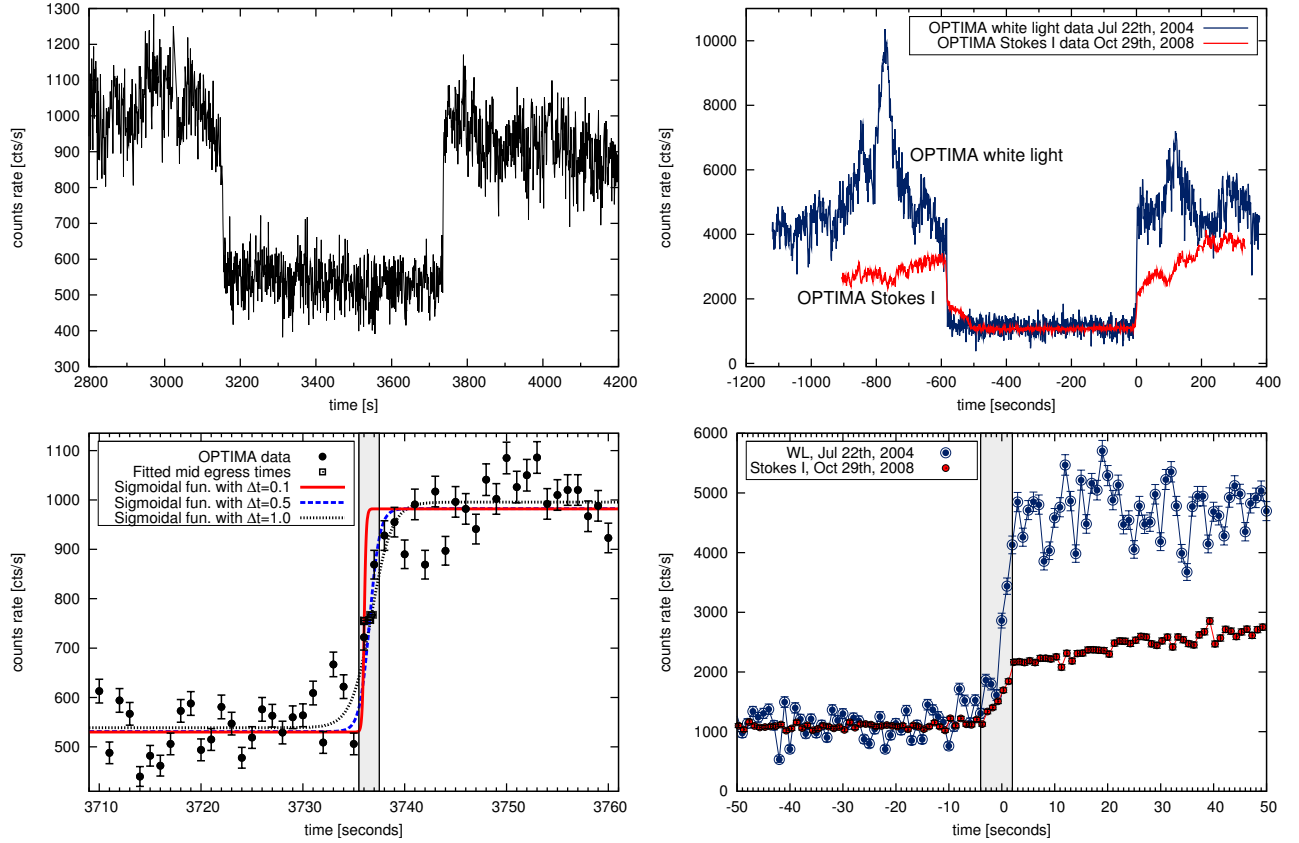


**Figure 5.** High time resolved OPTIMA light curves of HU Aqr. *The upper left panel:* photometric eclipse in the white light. *The bottom left panel:* a close-up around the mid-egress overlapped with three fitted sigmoid functions with different values set for the  $\Delta t$  parameter (0.1, 0.5, 1.0, respectively). The fitted mid-egress times are denoted by open squares. The shaded region corresponds to a time span of 2 seconds. *The upper right panel:* a comparison of photometric and polarimetric OPTIMA light curves of HU Aqr obtained in 2004 and 2008, respectively. *The bottom right panel:* a close-up of photometric and polarimetric HU Aqr light curves around the mid-egress time showing the difference between the egress shapes. The shaded region covers 6 seconds.

**Table 3.** Technical data of the MONET/N, PIRATE and TCS observations of HU Aqr.  $T_{\text{obs}}$  represents the observation time span, and  $\Delta T$  is the mean exposure time of a single frame.

Date	Instrument	Filter	$T_{\text{obs}}$ [hours]	$\Delta T$ [s]
2010 Oct 06	PIRATE	WL	1	10
2010 Oct 19	PIRATE	WL	3.5	10, 20
2011 Sep 30	TCS/WFC	WL	1	3
2011 Oct 01	TCS/WFC	WL	1	5
2011 Apr 03	MONET/N	WL	0.60	8
2011 May 03	MONET/N	WL	0.50	8
2011 Jul 21	MONET/N	WL	0.32	8
2011 Aug 17	MONET/N	WL	0.60	8
2011 Aug 20	MONET/N	WL	0.46	8
2011 Aug 20	MONET/N	WL	0.10	8
2011 Aug 21	MONET/N	WL	0.58	8
2011 Oct 22	MONET/N	WL	0.25	8
2011 Oct 23	MONET/N	WL	0.50	8
2011 Oct 25	MONET/N	WL	0.16	8
2011 Nov 18	MONET/N	WL	0.45	8

To derive the mid-egress moments gathered in Table 2, the sigmoid function was fitted to all single light curves.

### 4.3 On the light curves in different spectral windows

Vogel et al. (2008) and Vogel (2008) obtained high time resolved and accurate light curves of HU Aqr during its low state using the ULTRACAM (Beard et al. 2002; Dhillon et al. 2007) at the Very Large Telescope (VLT, May 13, 2005). These authors decomposed the light curve into three emission components emerging from the accretion spot, the photosphere surrounding it, and from the white dwarf itself. As a result, they were able to derive the temperature of the WD  $\sim 13500(200)$  K and the temperature of the accretion spot  $\sim 25500(1500)$  K. They also estimated the ratio of the spot area to the WD surface to be on the level of 5%. The black body spectra of the WD and of the spot have their maxima at 215 nm and 113 nm, respectively. The accretion spot and the accretion stream are time variable in brightness, as well as in the geometric position in the system. Therefore, the orbital phase at which they occur is not constant. The ULTRACAM delivers simultaneous light curves in three colours:  $u$ ,  $g$  and  $r$ . An example of such a three colour HU Aqr light curve can be found in Fig. 6 of Schwarz et al. (2009), where the shape—energy dependence can be easily seen. Thus, a comparison of egress times in different wavelength domains was possible. In the two cases with filters  $u$  and  $r$ , the WD constitutes the main contribution to the egress intensity, because it can be seen unperturbed when it comes out of eclipse. However, during high and intermediate accretion states, the WD might be out-shined by the accretion stream. In the  $u$ -band, the spot contributes 25% of the emission,

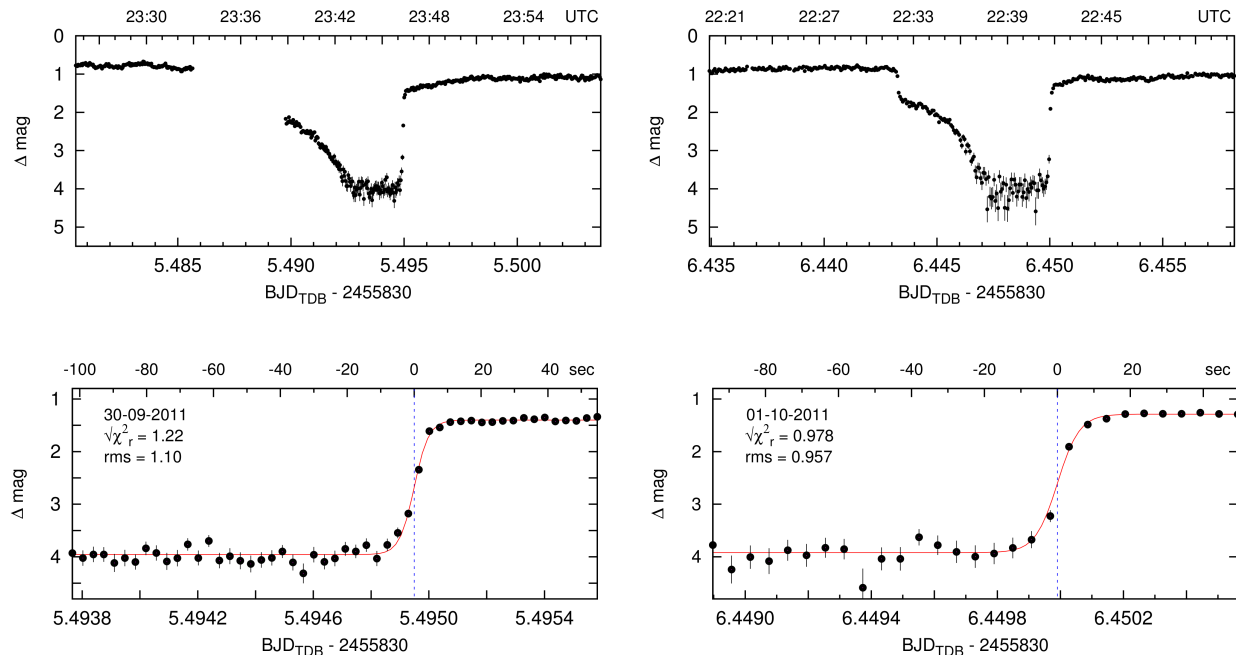


**Figure 6.** HU Aqr eclipse light curves obtained with the WFC mounted on the TCS. Observations were performed on 30/09/2011 and 01/10/2011 with integration times of 3 and 5 seconds, respectively. Bottom panels are for the close-up of eclipse egress, with fitted sigmoid function (solid line, see Eq. 12). Blue vertical lines mark the determined mid-egress times.

while in the  $r$ -band its contribution is only 12% (Vogel et al. 2008; Vogel 2008). This suggests that as the time marker of the eclipse, it is better to use more “reddish” than “blueish” data, particularly in our case as we have broadband observations gathered in X-rays, UV and optical domains at our disposal.

There exists evidence that the EUVE light curves differ from quasi-simultaneous ROSAT/HRI light curves, as it can be seen, for example, for eclipses recorded on October 1996 and May 1997, as shown in Fig. 2 of Schwöpe et al. (2001). The eclipse ingress is often not measured because of strong suppression of soft X-rays by absorbing matter along the accretion stream. When the eclipse duration can be determined, the eclipse duration seems shorter in the case of EUVE data. Thus the derived mid-egress moments can be shifted by a few seconds. According to Schwöpe et al. (2001), an expected variation of the eclipse span should be not more than 0.001 of the orbital phase which corresponds to not more than  $\sim 8$  seconds. Also Schwöpe et al. (2004) show in their Fig. 3 evidence of a different eclipse length as well as phase folded egress shapes at soft X-rays, HST UV, and high-speed optical photometry with a multichannel multicolor photometer (the MCCP 2.2 m telescope at Calar Alto) during the 1993 high state and the 1996 low accretion state. The scatter of the egress times resulting from changes of the accretion geometry during high and intermediate accretion states is estimated on the level of 2 seconds (Schwarz et al. 2009). Large differences between light-curves due to the eclipse of the accretion stream are also visible in the optical photometric measurements performed in parallel with the ROSAT observations (see Fig. 3 in Schwöpe et al. 2001). Some of those light curves were obtained with rather poor time resolution, e.g. 53 and 12 seconds.

It is worth mentioning that time stamps calculated by Schwöpe et al. (2001) and Schwarz et al. (2009) for the photon counting UV and X-ray detectors were computed from the mean of the arrival

times of the first three photons after the eclipse, while for the optical observations, they used the moments of the egress half intensity, which is common in the literature. Examples of the HU Aqr light curves obtained by the XMM-Newton EPIC-PN and Optical Monitor detectors are presented in Figures 2, 3 and 4 of Schwarz et al. (2009). XMM observations, contrary to the bright state ROSAT observations, were not resolved at time scales shorter than 2 seconds due to the low count rates.

We first used all available egress times, archival as well as new ones, to model the (O-C) diagram. However, given the above-mentioned arguments, we decided to select only those measurements that were obtained in the white light or photometric V band, in order to keep the data more uniform and homogeneous. This approach renders the measurements independent of possible varying emission regions in different bands. We also decided to skip the most “suspicious” egress-times at some stage of fitting the orbital model, which is described below.

We note that the HST observations (three points around  $l \sim 14,000$ ) were performed with the FOS instrument in the 120–250 nm range. These points were also excluded in our further analysis, falling out of the white light and the V band range.

## 5 MODELING ALL RECENT DATA

Thanks to the new set of precision OPTIMA mid-egress measurements, as well as observations performed at PIRATE, TCS and MONET/N telescopes, we can re-fit planetary models to the whole set of data up to November 18th, 2011. We fitted the data with the linear and quadratic ephemeris models (Eqs. 10, 11).

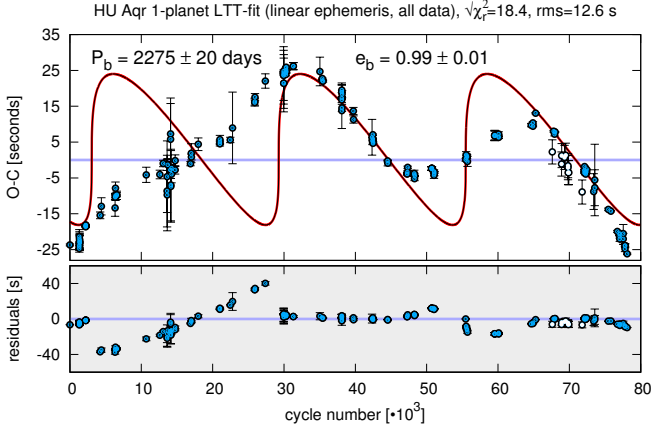


**Figure 7.** Synthetic curve of the 1-planet LTT model with linear ephemeris to all available data, including the very recent egress times collected by the OPTIMA photometer, as well as PIRATE, TCS and MONET/N telescopes. Open circles are for measurements in Qian et al. (2011).

### 5.1 Single-planet models to all recent data

At the first attempt, we tested the 1-planet hypothesis. For the linear ephemeris model, the 1-planet solution is characterized by extreme eccentricity and displays large residuals and a strong trend present in the (O-C) diagram (see Fig. 7). This suggests a more general quadratic model, on which we focus now.

The results derived for the whole set of 171 measurements are shown in the top panels of Fig. 8. Interestingly, the 1-planet model fits the data very well in a large part of the time-window between  $l = 25,000$  and  $l = 80,000$  (see the left-hand panel of Fig. 8). However, over approximately one fourth of the time-window ( $l = 0$  to  $l = 25,000$ ), the data fit the synthetic curve poorly. That can be better seen in the close-up of the residuals shown in the top right panel of Fig. 8. It appears that the residuals follow a regular and characteristic “damping” trend, that could be associated with a mass-transfer process ongoing in the binary or solar-like magnetic cycles. Results of our experiments show that the recent observations by Qian et al. (2011) appear to be outliers to our 1-planet solution, as the mid-egress times are shifted by about of 3–10 seconds w.r.t. the synthetic curve. Because these observations overlap in the time window with much more precise OPTIMA data, that discrepancy between these two data sets cannot be avoided. Actually, observations by Qian et al. (2011) do not fit any model that has been tested with the OPTIMA observations, including 2-planet models and both types of the ephemeris (see the Appendix).

In an effort to explain the strange behaviour of the residuals, we realized, as it was discussed already, that the available observations come from different telescopes/instrumentation, and to make the matter worse, the egress times are measured on the basis of light curves in different spectral windows. In particular, the first part of the data set contains the egress times derived from X-rays (ROSAT and XMM) and ultraviolet (EUVE, XMM OM-UVM2 and HST/FOS) light curves, and some eclipses were observed with OPTIMA in polarimetric mode. To remove the possible inconsistency due to the different spectral windows and filters, we considered data sets consisting of the egress times measured only in the optical range (white light and the V band). The results are shown in the bottom panels of Fig. 8 for the optical data *without* X-ray and UV, but *including* polarimetric measurements (note, that the polarimetry was done in the white-light band; compare with the

**Table 4.** Keplerian parameters for the 1-planet LTT fit model with quadratic ephemeris to all data gathered in this work (Fit I) and to measurements selected in the optical and V-band domain (Fit II). Synthetic curves with mid-egress times overplotted are shown in Figs. 8 and 9. Numbers in parentheses represent the uncertainty at the last significant digit. Total mass of the binary is  $0.98 M_{\odot}$  (Schwope et al. 2011). See the text for more details.

Model parameter	Fit I all measurements	Fit II optical measurements
$K_b$ [seconds]	$13.9 \pm 0.3$	$14.7 \pm 0.2$
$P_b$ [days]	$3278 \pm 28$	$3287 \pm 19$
$e_b$	$0.03 \pm 0.04$	$0.13 \pm 0.04$
$\omega_b$ [degrees]	$211 \pm 40$	$226 \pm 10$
$T_b$ [BJD 2,440,000+]	$6233 \pm 360$	$6361 \pm 102$
$P_{bin}$ [days]	0.0868204226(5)	0.0868204259(4)
$T_0$ [BJD 2,440,000+]	9102.92004(2)	9102.91994(1)
$\beta$ [ $\times 10^{-13}$ day cycle $^{-2}$ ]	-2.61 (5)	-2.95(4)
$a_b$ [au]	4.29	4.30
$m_b \sin i$ [ $M_{Jup}$ ]	6.71	7.10
$N$ data	171	115
$(\chi^2_{\nu})^{1/2}$	5.23	2.48
rms [seconds]	4.8	3.7

top panels of Fig. 8 for all data gathered). As can be seen from the bottom panels in Fig. 8, the “damping” effect has almost vanished, suggesting that it could have appeared due to the presence of X-ray and UV-derived eclipses. Still, there is a group of data points with large errors, around  $l \sim 14,000$ , which do not fit well to the clear quasi-sinusoidal variation of the (O-C). The deviations of these points may be explained by poor time-resolution ( $\sim 12$  seconds of the AIP07 CCD camera), that has been used to observe the HU Aqr eclipses (Schwope et al. 2001). Let us also note that the Qian et al. (2011) data points are again systematically outliers with respect to the synthetic signal. After removing these data and all points (seven measurements) in the polarimetric mode, we obtained a homogeneous optical data set to which we fitted the quadratic ephemeris 1-planet model again. The synthetic curve of this fit with data points over-plotted is shown in Fig. 9. Parameters of this fit are presented in Table 4 as the final solution Fit II and are well constrained by the observations. To demonstrate the latter, we show projections of  $(\chi^2_{\nu})^{1/2}$  in selected two-dimensional parameter-planes (see Fig. 10) close to the best-fit model. As can be seen, there is a strong correlation between the time and argument of pericentre which can be understood noting that the orbital phase ( $\lambda_b = \omega_b + M_b$ ) must be preserved.

The best-fit model seem to constrain the damping factor  $\beta \sim -3 \times 10^{-13}$  day cycle $^{-2}$  very well. Such a value is close to estimates in the literature, e.g.,  $\sim -5 \times 10^{-13}$  day cycle $^{-2}$  by Schwarz et al. (2009) and  $\sim -2.5 \times 10^{-13}$  day cycle $^{-2}$  by Qian et al. (2011). It is still larger by more than one order of magnitude to be explained by gravitational radiation, but remains in the range of magnetic braking (Schwarz et al. 2009). A similar large-magnitude period decrease has been found in other CVs, like NN Ser ( $\sim -6 \times 10^{-13}$  day cycle $^{-2}$ , Brinkworth et al. 2006). Besides the angular momentum loss, the large magnitude of the period change is commonly explained as due to the Applegate mechanism (basically excluded in the HU Aqr) and/or a the presence of a very distant, long-period companion body. Likely, a few astrophysical and/or dynamical effects may be involved that could determine ap-

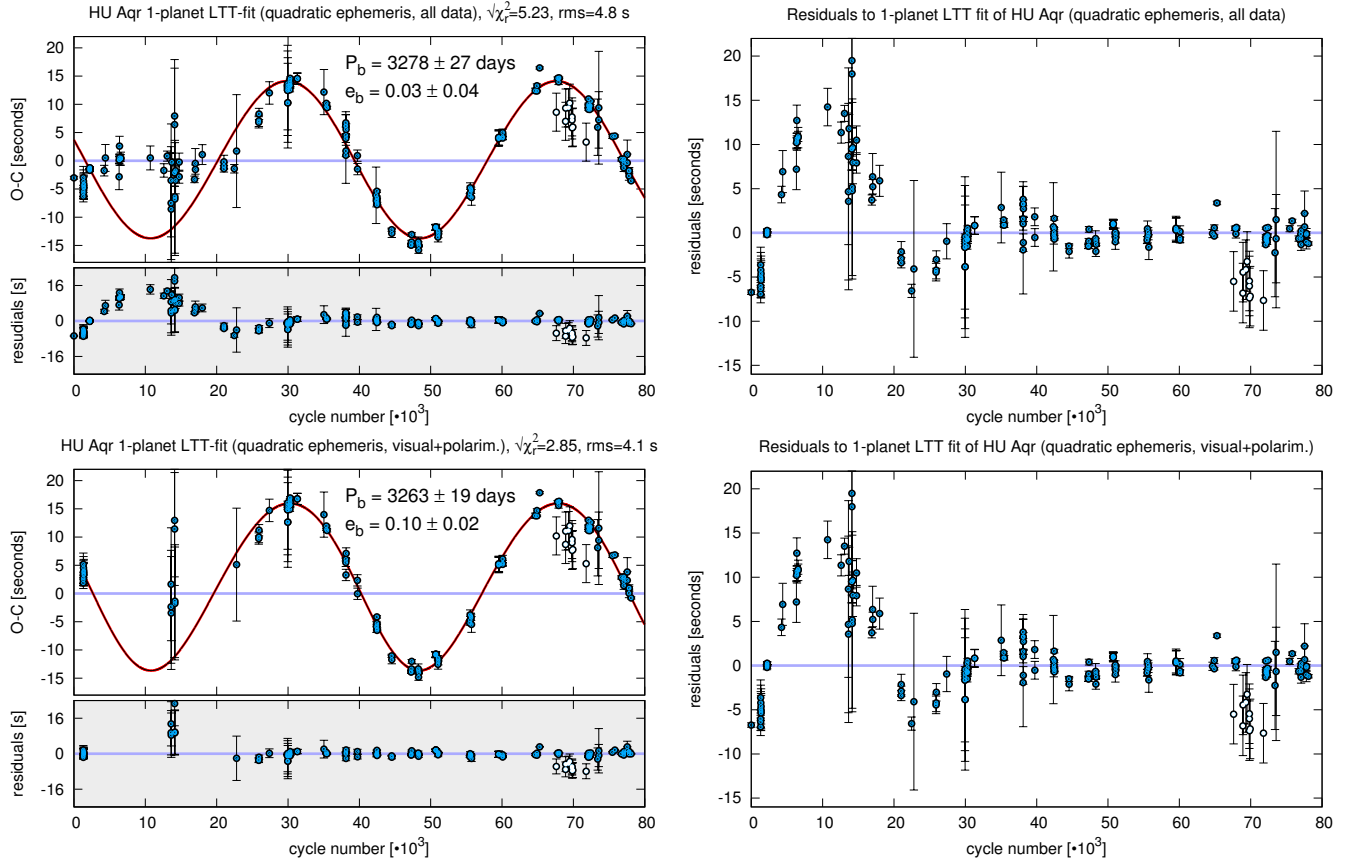


**Figure 8.** *The top row:* synthetic curve of the 1-planet LTT model with quadratic ephemeris to all available data, gathered in this work, including the very recent mid-eclipse times collected by the OPTIMA photometer, as well as PIRATE, TCS and MONET/N telescopes (*the top left*) with orbital parameters given in Table 4 (Fit I), and close-up of residuals to that model (*the top right panel*). *The bottom row:* the same for the white light and visual band (V) data, including polarimetric observations by OPTIMA (i.e., the UV- and X-band observations are excluded) shown at *the bottom left panel*, and its residuals (*the bottom right panel*). The white filled circles mark the Qian et al. (2011) measurements.

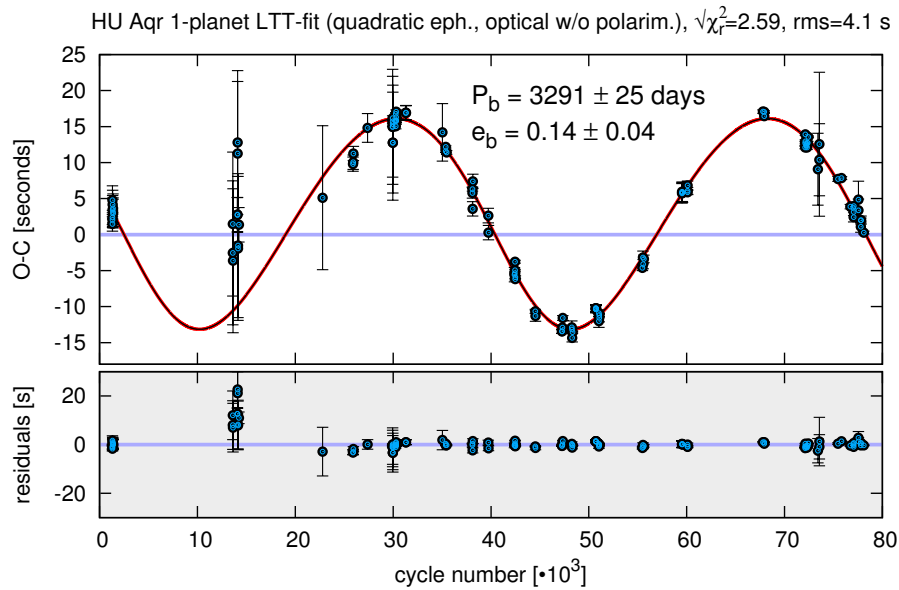


**Figure 9.** Synthetic curve of the 1-planet LTT model with quadratic ephemeris to observations in white light + V band (see the text for more details) *without* measurements in Qian et al. (2011) and polarimetric data. Orbital parameters of this solution are given in the Table 4 (Fit II).

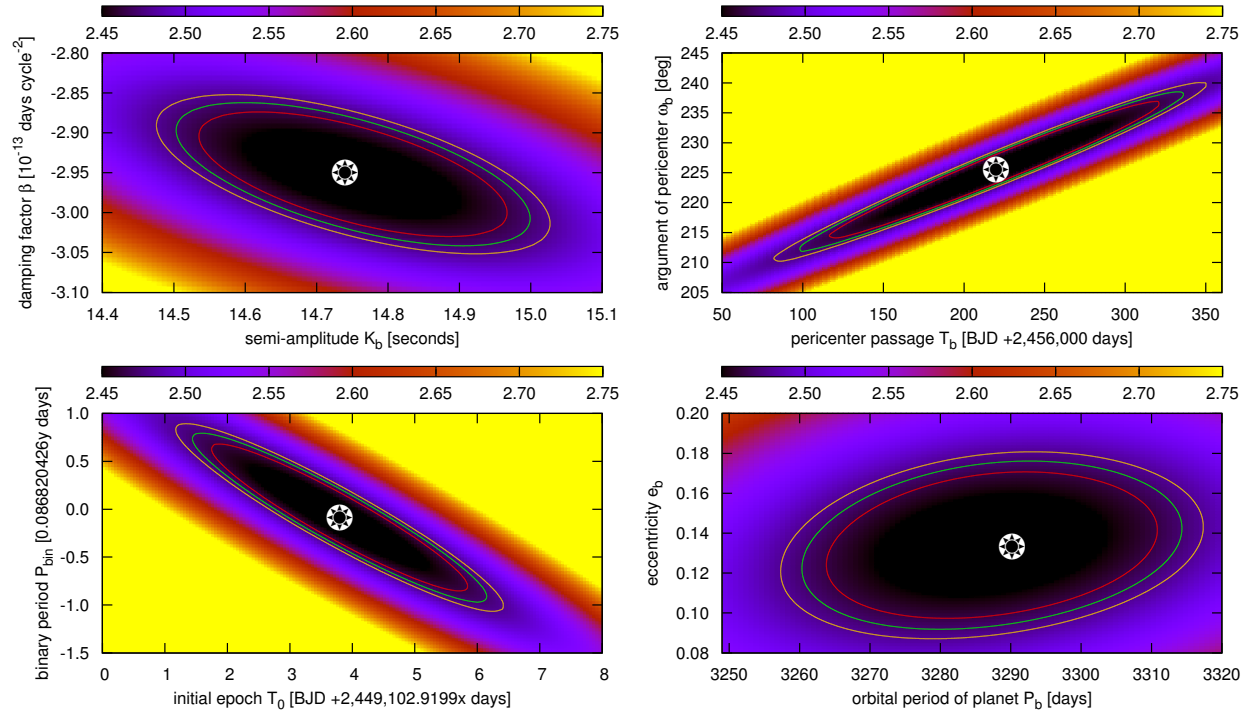


**Figure 10.** Colour-coded parameter scans of  $(\chi_v^2)^{1/2}$  around the best-fit 1-planet model, to quadratic ephemeris and the optical measurements (Fit II in Table 4). Its synthetic curve with data points overplotted is shown in Fig. 9. The large symbol marks nominal elements of the solution. Closed curves are for formal 1, 2, 3 $\sigma$  levels of  $(\chi_v^2)^{1/2}$  with scale displayed at the colour legend.

parently secular period decrease. Its definite explanation is complex, and we consider this as a subject of a new, forthcoming work.

We also fitted the quadratic ephemeris model only to the high-precision OPTIMA data. The results for measurements that include polarimetric observations are shown in Fig. 11. For that case, we found a period similar to the quadratic ephemeris model for the entire data set. The fit has very small rms  $\sim 0.8$  sec. The relatively large  $(\chi_v^2)^{1/2} \sim 3.4$  of the OPTIMA solution in this case may suggest that the adopted uncertainties, at the  $\sim 0.1$ – $0.2$  second level (in a large sub-set of the measurements) are in fact underestimated. We also identified the most deviating points as coming from the polarimetric measurements (see e.g., a point marked in the residuals plot around  $l = 65,000$ , and the residuals of both solutions). To examine, whether these data may change the solution, we fitted the quadratic ephemeris model to the white light OPTIMA observations only, skipping all polarimetric data. The best-fit orbital period of  $\sim 3400$  days remains close to the full-coverage window fit. A slightly smaller rms of  $\sim 0.7$  seconds suggest a better fit without the polarimetric data, indeed. The orbital periods coincidence cannot be fully proved due to the relatively narrow observational window of the OPTIMA white light measurements. Actually, the parameter scan (not shown here) reveals that the 1 $\sigma$  contour around the  $(\chi_v^2)^{1/2}$  minimum in the  $(P_b, e_b)$ -plane is “opened” on the right side of the orbital period-axis, hence it can not be constrained yet by the OPTIMA data alone.

## 5.2 Alternate models to all recent data

Finally, using the hybrid optimiser, we performed additional experiments by fitting three models to all available data: the 1-planet model with a heuristic sine damping term, and 2-planet models, both in terms of the linear and quadratic ephemeris. We also per-

formed  $N$ -body modeling of the 2-planet configurations. The results, which are described in the Appendix, imply that all these models lead to non-unique solutions or configurations with similar orbital periods, for which the kinematic model is inadequate, as we discussed above. Some of these kinematic best-fit 2-planet solutions are qualitatively similar to configurations found for the SSQ data set, with orbital periods ratios close to 1c:1b and 4c:3b, respectively. The extended data set still does not constrain the Keplerian 2-planet models.

The same can be concluded for the  $N$ -body models (see Appendix, Sect. A3). Although we found *stable* configurations in terms of the quadratic ephemeris, the semi-major axis of the outer companion is unconstrained (between 4 AU and at least 20 AU). These stable fits exhibit varying sign of  $\beta$  (it means that the binary period might decrease or increase). Moreover, stable solutions with relatively small  $\beta$  may be found in very narrow stability zones in the  $(a_c, e_c)$ -plane, see the Appendix and Fig. A6. These areas are associated with low order MMRs, like 3c:2b MMR. It is very uncertain though, how massive companions of HU Aqr could be locked in such tiny stability areas. Hence, some larger values of  $a_c$  providing extended zones of stable motions seems more likely (see panels of stable fits labeled by IV, V, and VI of Fig. A6). However, there is also a correlation between the magnitude of  $\beta$  and the semi-major axis of the outer planet. For relatively distant planet c,  $|\beta|$  may be  $\sim 2 \times 10^{-12}$  day cycle $^{-2}$ , which is difficult to explain by magnetic braking or mass-loss. However, this may indicate a presence of a third companion in an unconstrained orbit.

We conclude that these results seem to favour the 1-planet hypothesis as the simplest model explaining the (O-C) variability, particularly in the light of very small rms of the homogeneous OPTIMA set and apparently perfect quasi-sinusoidal fit illustrated in Fig. 11.

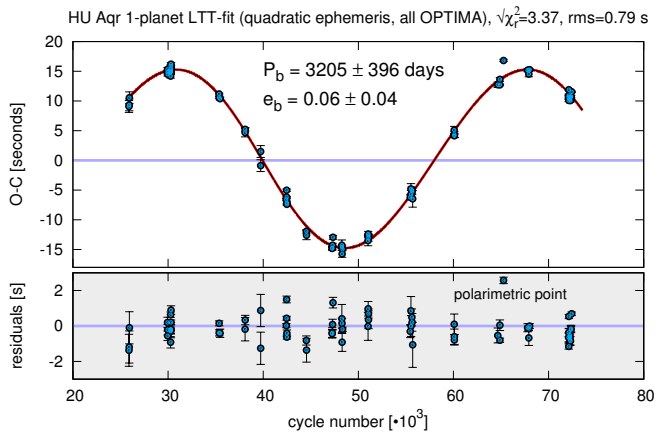


**Figure 11.** Synthetic curves of the 1-planet LTT quadratic ephemeris models to optical OPTIMA measurements, including polarimetric data. One of the most deviating polarimetric points is labeled in the residuals panel.

## 6 RED NOISE AND/OR SYSTEMATIC ERRORS?

Analysis of the LTT observations has much in common with pulsar timing, planetary transits, and precision radial velocity observations, which are modelled with least-squares under the assumption that the measurement errors are uncorrelated (white noise). However, as is known particularly by pulsar observers, the assumption that white noise is the only source of error is unjustified when aiming at estimating the underlying model parameters and their uncertainties (Coles et al. 2011). In the past, this effect had been responsible for false detections of planets around pulsars (Bailes et al. 1991). Similarly, correlated (red) noise or systematic errors have been found in the planetary transit data (Pont et al. 2006) and very recently, in the radial velocity measurements (Baluev 2011). The same type of non-Gaussian, low-frequency correlation of residuals to the orbital period of the binary may be present in the LTT data collected over long time intervals.

The danger of such systematic effects in the LTT-analysed binaries is reinforced due to their activity and complex astrophysical phenomena responsible for the observed emission. One of the already well recognized mechanisms able to produce cyclic variation of the orbital period of the binary has been proposed by Applegate (1992). As shown by this author, a magnetic star (here, the secondary) changes its internal structure due to magnetic cycles. The latter implies a variable zonal harmonic coefficient  $J_2$  and subsequently, a variable gravitational tidal field for the orbital companion which results in a varying orbital period (Hilditch 2001). The Applegate mechanism as a possible origin of large (O-C) variations in the HU Aqr data was studied in detail by Vogel (2008), as well as by Schwarz et al. (2009). They discarded this possibility since the HU Aqr stellar setup does not provide enough energy to drive changes of the orbital period. Similar results were obtained for the NN Ser system, that likewise has a low-mass, low-luminosity secondary star (Brinkworth et al. 2006) with a conclusion that it is incapable of driving significant period changes in terms of the Applegate model.

Another mechanism explaining observed long-term periodicities could be a slow precession of the rapidly spinning magnetic WD star, which has been proposed as a source of long periods detected in a few CVs, for instance FS Aur and V455 And (Tovmassian et al. 2007). However, HU Aqr is unlikely to host such a WD, as this AM Her-like system is known to be synchronously locked.

As a first, yet preliminary attempt, we tried to determine the characteristic that can be used to quantify the shapes of the HU Aqr light curves and might help to detect their variability and hence astrophysical sources of the LTT residuals. This approach mimics the bisector velocity span (BVS) technique used to detect distortion of spectral lines due to stellar spots and chromospheric activity. It is well known that stellar spots may produce apparent radial velocity changes up to  $200 \text{ ms}^{-1}$  (Berdyugina 2005). As a similar characteristic to the BVS, we choose the slope of the linear function fitted to the egress phase of the light curve, usually spanning no more than a few seconds interval. We analysed 59 available light curves in the precision OPTIMA set. The results are shown in Fig. 12. In seven cases, we decided the data were not precise enough to derive the slope reliably (as indicated by green filled squares) because of, for instance, bad weather or strong wind that could introduce telescope guidance errors. In a few other cases (seven again, marked with blue triangles), only two points were taken for the fit, and therefore no error estimation was possible. Nevertheless, the obtained slopes are uniform and span less than 2 degrees range close to 90 degrees. That furthermore indicates a similarly rapid egress phase. The results of this test are encouraging, and support the planetary hypothesis.

However, the slopes should be best re-computed for all available light curves that were used to determine the egress-times. The problem of the non-homogeneity of the collected light curves still exists. Due to varying eclipse profiles (e.g. during different accretion states), the determination of mid-egress dates is often very difficult. For instance, it could be prone to rather subjective choices of the photometric data range to fit the parameters of the sigmoid function, Eq. 12. That may introduce significant systematic errors, particularly if the reduction is performed by different researchers. This issue may be likely resolved by a re-analysis of the entire set of all available light curves, under similar conditions paying particular attention to their origin – the spectral window, an instrument, and even technical and observational circumstances.

Another direction still open is a study of the binary interactions, to eventually eliminate or discover astrophysical causes of the LTT variability. The problem is in fact universal and affects other techniques of extrasolar planets detection, such as pulsar timing and radial velocity monitoring of active or evolved stars, as well. It is yet possible that the observed (O-C) signal has both the planetary and unmodeled astrophysical component (Potter et al. 2011), making its unique resolution even harder.

To the best of our knowledge, possible effects of the red-noise regarding the LTT observations have not been studied in detail. That problem certainly deserves a deep and careful investigation.

## 7 CONCLUSIONS

Using a new formulation of the LTT model of the (O-C) to the available data of the HU Aqr system, we found that the 2-planet hypothesis by Qian et al. (2011) is not likely. Our results reinforce recent negative tests of dynamical stability of that system in the literature. The self-consistent LTT model presented in this work exhibits degenerate solutions, such as (apparently) Trojan objects of  $\sim 10^4$  Jupiter masses, or a companion in an collisional/open parabolic or hyperbolic orbit. Ironically, two such solutions to the literature SSQ data are the best-fit models found in extensive, quasi-global searches adopting a hybrid optimization.

Moreover, on the basis of a much extended, precision data set, collected by the OPTIMA network, that increased the number of

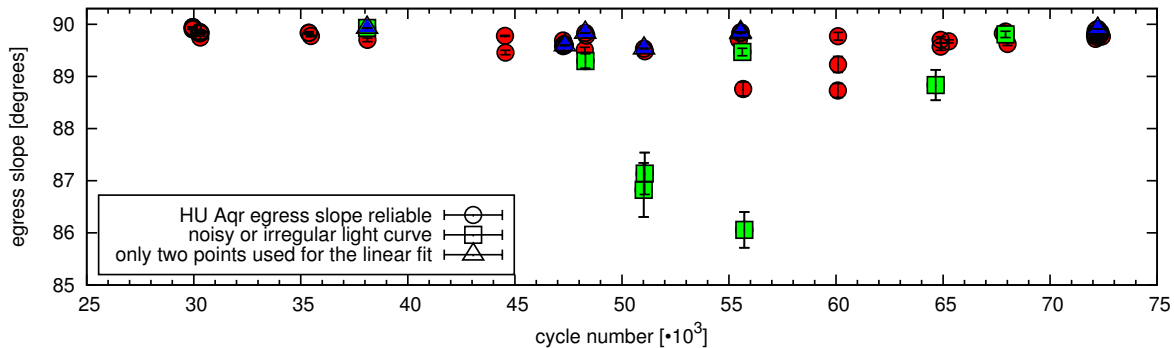


**Figure 12.** Linear slopes of 59 HU Aqr egresses derived on the basis of OPTIMA light curves by fitting a linear function only to the egress phase, usually spanning not more than a few seconds. In seven cases, the light curves were not precise enough (as indicated by green filled squares) because of a bad weather. In other seven cases, only two points were taken for the fit, therefore no error estimation was possible (blue triangles). See the text for more details.

data points analysed in previous works by  $\sim 50\%$ , we have shown that the observed (O-C) variations may be consistently explained by the presence of only one circumbinary planet of the minimal mass of  $\sim 7$  Jupiter-masses, in an orbit with a small eccentricity of  $\sim 0.1$  and an orbital period of  $\sim 10$  years, similar to Jupiter in the Solar system. Our results support the original 1-planet hypothesis by Schwarz et al. (2009) rather than the 2-planet model proposed by Qian et al. (2011). If confirmed, that planet would be the next circumbinary object detected from the ground, shortly after such companions have been announced around HW Vir (Lee et al. 2009), NN Ser (Beuermann et al. 2010), UZ For (Potter et al. 2011), SZ Her (Lee et al. 2011), DP Leo (Beuermann et al. 2011), followed by recent discoveries of Kepler-16b (Doyle 2011), Kepler-34b and Kepler-35b planets (Welsh et al. 2012). According to estimates by these authors, the observed rate of circumbinary planets around close binaries may be  $\sim 1\%$ .

Also, we found that the observations by Qian et al. (2011) are not confirmed by the OPTIMA measurements due to systematic relative shift of  $\sim 3$ – $10$  seconds. The nature of this discrepancy is yet unknown. If the shift is caused by an error, all 2-planet models presented in the literature that make use of their data are affected.

Besides the disagreement between our conclusions and the previous works, our results suggest that the kinematic modeling of 2-planet configurations is not fully justified on the grounds of the dynamics because the best-fit models may imply large masses (up to stellar range), large eccentricities, and similar orbital periods indicating a possibility of strong mean motion resonances. Moreover, the (O-C) variability that suggests 2-planet solutions most likely appears due to mixing observations done in different spectral windows. That feature of the data set – as we have shown here – introduces systematic effects that may alter the best-fit solutions significantly. This conclusion is supported by extensive numerical simulations of the 2-planet systems dynamics by Horner et al. (2011), Wittenmyer et al. (2012) and Hinse et al. (2012). Considered within statistical error ranges, the initial conditions lead to catastrophically disruptive configurations, unconstrained elements of the outermost body, and/or period damping factor  $\beta$ .

In this work, we found best-fit stable 2-planet models within the quadratic ephemeris  $N$ -body model to *all available data*, but the semi-major axis of the outer planet cannot be yet constrained. Stable configurations are located within low-order MMRs spanning tiny stable zones in the phase space, or are characterised by a large magnitude of the period decrease. In the first case, it is difficult to explain, how a few Jupiter mass companions could be trapped

in such particular, isolated resonances. In the second case, a large  $|\beta|$  requires an efficient, internal mechanism of the binary period change, or indicates a presence of one more companion. Our findings might be a breakthrough after a few cited works reporting basically only unstable 2-planet models of the HU Aqr system, but these discrepancies add even more ambiguity to the 2-planet hypothesis.

However, the results of our experiments show that the 1-planet solution is relatively well constrained by available *optical observations* selected as a homogeneous data set. Because the early optical data (the white light and V-band measurements) are coherent with an impressive, very clear quasi-sinusoidal signal exhibited by superior-precision OPTIMA measurements, as well as with the recent MONET/N, PIRATE and WFC data, a single-companion hypothesis seems well justified. A confirmation of the planetary origin of the LTT signal still requires long-term monitoring of the system. Due to its very long orbital period, it will take many years to confirm or reject the signal coherence. Such new data would be also very useful to constrain the orbital period by the recent OPTIMA observations alone.

**Acknowledgements.** We thank the anonymous referee for a review and comments that improved the manuscript. We would like to thank Maciej Konacki (CAMK Toruń) for a discussion and a suggestion of the egress slopes test, as well as Anna Zajczyk (CAMK, Toruń), Andrzej Szary (UZG, Zielona Góra), Alex Stefanescu, Martin Mühlegger, Helmut Steidle, Natalia Primak, Fritz Schrey, and Christian Straubmeier (all MPE) for their help with observations. Krzysztof Goździewski is supported by the Polish Ministry of Science and Higher Education Grant No. N/N203/402739 and POWIEW project of the European Regional Development Fund in Innovative Economy Programme POIG.02.03.00-00-018/08. İlham Nasiroglu acknowledges support from the EU FP6 Transfer of Knowledge Project “Astrophysics of Neutron Stars” (MKTDC-CT-2006-042722). Aga Słowikowska would like to thank Bronek Rudak for his support and discussions. She also acknowledges support from the Foundation for Polish Science grant FNP HOM/2009/11B, as well as from the Marie Curie European Reintegration Grant within the 7<sup>th</sup> European Community Framework Programme (PERG05-GA-2009-249168). Gottfried Kanbach acknowledges support from the EU FP6 Transfer of Knowledge Project ASTROCENTER (MKTDC-CT-2006-039965) and the kind hospitality of the Skinakas team at UoC. B. Gauza thanks the Wide FastCam team for help in performing the observations. Research by Tobias C. Hinse is carried out under the KRCF Young Researcher

Fellowship Program at the Korea Astronomy and Space Science Institute. NH acknowledges support from the NASA Astrobiology Institute under Cooperative Agreement NNA09DA77A at the Institute for Astronomy, University of Hawaii, and from NASA/EXOB program under grant NNX09AN05G. We thank the Skinakas Observatory for their support and allocation of telescope time. Skinakas Observatory is a collaborative project of the University of Crete, the Foundation for Research and Technology – Hellas, and the Max-Planck-Institute for Extraterrestrial Physics. This article is based on observations made with the TCS telescope operated on the island of Tenerife by the Instituto de Astrofísica de Canarias in the Spanish Teide Observatory. This work is based in part on data obtained with the MOnitoring NETwork of Telescopes (MONET), funded by the Alfred Krupp von Bohlen und Halbach Foundation, Essen, and operated by the Georg-August-Universität Göttingen, the McDonald Observatory of the University of Texas at Austin, and the South African Astronomical Observatory.

## APPENDIX A: ALTERNATE MODELS TO ALL DATA

In this section, we display supplementary results illustrating a few alternative models to the 1-planet solution of the (O-C) of the HU Aqr binary that was analysed in the main part of the paper. Basically, all 171 data points are modeled, although in some cases, we removed outlying data from Qian et al. (2011) because they clearly introduce a systematic error. We considered 1-planet model with a heuristic, sine-damping term (Sect. A1), 2-planet kinematic models (Sect. A2) and the full, 2-planet, self-consistent Newtonian model (Sect. A3). The aim of this Appendix is to demonstrate that 2-planet models lead to non-unique or unconstrained solutions. Hence, these results reinforce a hypothesis of a single, quasi-sinusoidal signal of possibly planetary origin.

### A1 Quadratic ephemeris 1-planet model with damping term

To describe the suggested damping signal visible in Fig. 8 (the top right-hand panel), we modified the quadratic ephemeris model by adding a heuristic term having the following form:

$$\tau_{\text{damp}}(t) = \tau_0 + A \exp(-t/T_{\text{damp}}) \sin(n_{\text{damp}}t + \phi_0), \quad (\text{A1})$$

where  $\tau_0$  is an offset,  $A$  is the semi-amplitude of the signal,  $T_{\text{damp}}$  is the damping time scale,  $n_{\text{damp}} = 2\pi/P_{\text{damp}}$  is the frequency, and  $\phi_0$  is the initial phase at epoch  $t = 0$ . Two examples of best-fit solutions to all available data (171 measurements) are shown in Fig. A1. Let us note that the planetary orbital period in the configuration in the right-hand panel of this figure is twice the period in the 1-planet model studied earlier. The (O-C) of a solution shown in the left-hand panel cannot be distinguished from 2-planet models (see the text below).

A physical nature of that damped signal is uncertain. Allowing for some speculations, the damping might appear due to a long-term relaxation in the binary system which may, for instance, be due to the binary's magnetic cycles (Applegate mechanism). In such a case, the observed LTT signal would be resulted from two distinct phenomena. However, we recall here that Vogel (2008) and Schwarz et al. (2009) estimated that the Applegate mechanism cannot be responsible for orbital changes of HU Aqr.

### A2 Kinematic 2-planet models

We also tested 2-planet models with the linear and quadratic ephemeris, (Eqs. 10, 11). Examples of the best-fit configurations with comparable  $(\chi^2_{\text{v}})^{1/2}$  and an rms are shown in Fig. A2. Similar to the case of the SSQ data set, no unique solution may be found. For the parabolic ephemeris, we found many similar-quality best-fit solutions. These fits are characterised by the orbital periods ratio close to 1c:1b MMR with inferred planetary masses of  $\sim 20 M_{\text{Jup}}$  (the bottom left-hand panel in Fig. A2), close to 4c:3b MMR with inferred masses of  $\sim 5.5 M_{\text{Jup}}$  and  $\sim 4.0 M_{\text{Jup}}$  (the top right-hand panel in Fig. A2). A solution close to the 2c:1b MMR (the top right-hand panel in Fig. A2), as well as configurations with extreme eccentricity  $e_c \sim 0.95$ , positive damping factor  $\beta \sim 10^{-12}$  cycles day $^{-2}$ , and unconstrained  $P_c \sim 250,000$  days (not shown here) was also found. In all these cases, the rms remains at the level of 2.4 seconds. Some of these solutions are qualitatively similar to the 2-planet fits found for the SSQ data set. These results imply that the significantly extended data set still does not constrain 2-planet models.

For the linear ephemeris model, we found one best-fit solution that frequently appeared in different runs of the hybrid code. It is shown in the bottom right-hand panel of Fig. A2. This solution is characterised by an orbital periods ratio close to 6:5. Taken literally, this fit corresponds to Trojan brown dwarfs. However, the kinematic model is inadequate for such a configuration of massive objects.

### A3 Newtonian, self-consistent $N$ -body 2-planet models

In the light of the discussion presented above, we performed a preliminary modelling of all available data with the help of the hybrid algorithm driven by the self-consistent  $N$ -body model. Moreover, we tested Lagrange stability of the best-fit models following their orbital evolution over at least  $10^6$  orbital periods of the outermost planet. Configurations which survived during such time without a collision or remaining on closed orbits were regarded stable. In this experiment we use 161 data points, excluding data in (Qian et al. 2011), due to the discrepancy with OPTIMA measurements.

To illustrate the results of the hybrid optimization, we projected the found solutions onto particular planes of the Keplerian astrometric, osculating elements of the planets (Fig. A3) at the epoch of the first observation. The general finding is that the  $N$ -body formulation helps to improve the rms, that decreased from  $\sim 2.4$  seconds to  $\sim 1.9$  seconds as compared to kinematic models.

The top row of Fig. A3 illustrates the results for the linear ephemeris. Clearly, the data do not constrain the semi-major axes and eccentricities of the companions. The eccentricities tend to be large, up to 0.8. Moreover, the best-fit configuration exhibit similar values of semi-major axes ( $\sim 5.6$  AU and  $\sim 6.3$  AU) and large masses in the brown-dwarfs range of  $\sim 20$  Jupiter masses. We did not find any stable configurations within this model. It is consistent with the results for the SSQ data set (Hinse et al. 2012).

Interesting results are obtained for the quadratic ephemeris model (see the bottom row in Fig. A2) although also this model does not constrain orbital parameters, due to even larger spread of the semi-major axes and eccentricities than in the linear ephemeris model. Two minima of  $(\chi^2_{\text{v}})^{1/2}$  are found, around  $a_b \sim 4$  au, and  $a_b \sim 6$  au, respectively. The best-fit configurations have  $(\chi^2_{\text{v}})^{1/2} \sim 2.6$  and an rms  $\sim 1.9$  second that is  $\sim 20\%$  better than for the best kinematic models. In the neighborhood of the first  $(\chi^2_{\text{v}})^{1/2}$  minimum ( $a_b \sim 4$  AU), we found a few thousands of Lagrange

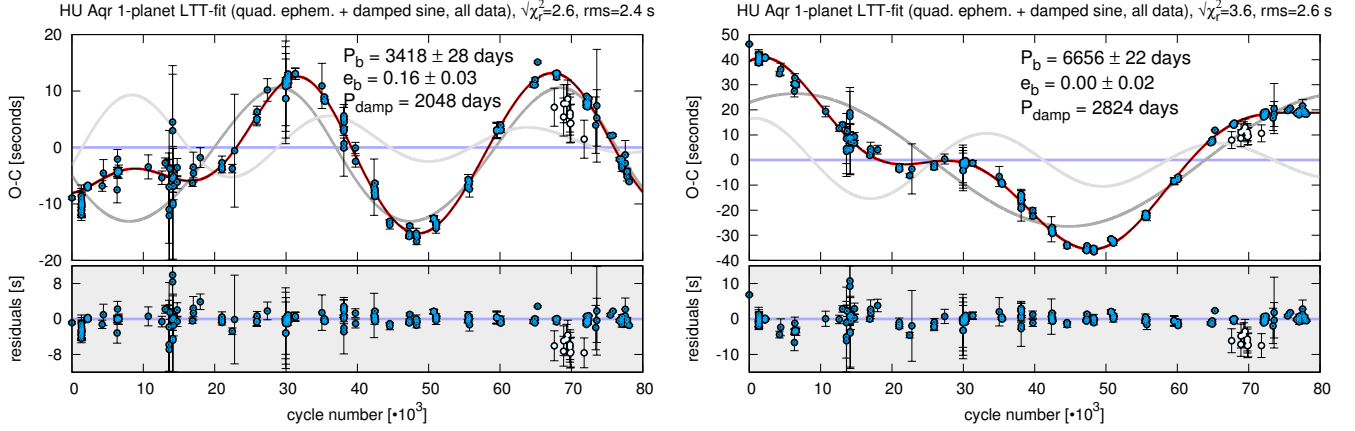


**Figure A1.** Examples of synthetic curves of the 1-planet LTT quadratic ephemeris models with a sine damping term to all 171 data points gathered in this work, including 10 measurements in Qian et al. (2011), marked with white filled circles. The shaded curves represent the planetary and the damped sine signal, respectively.

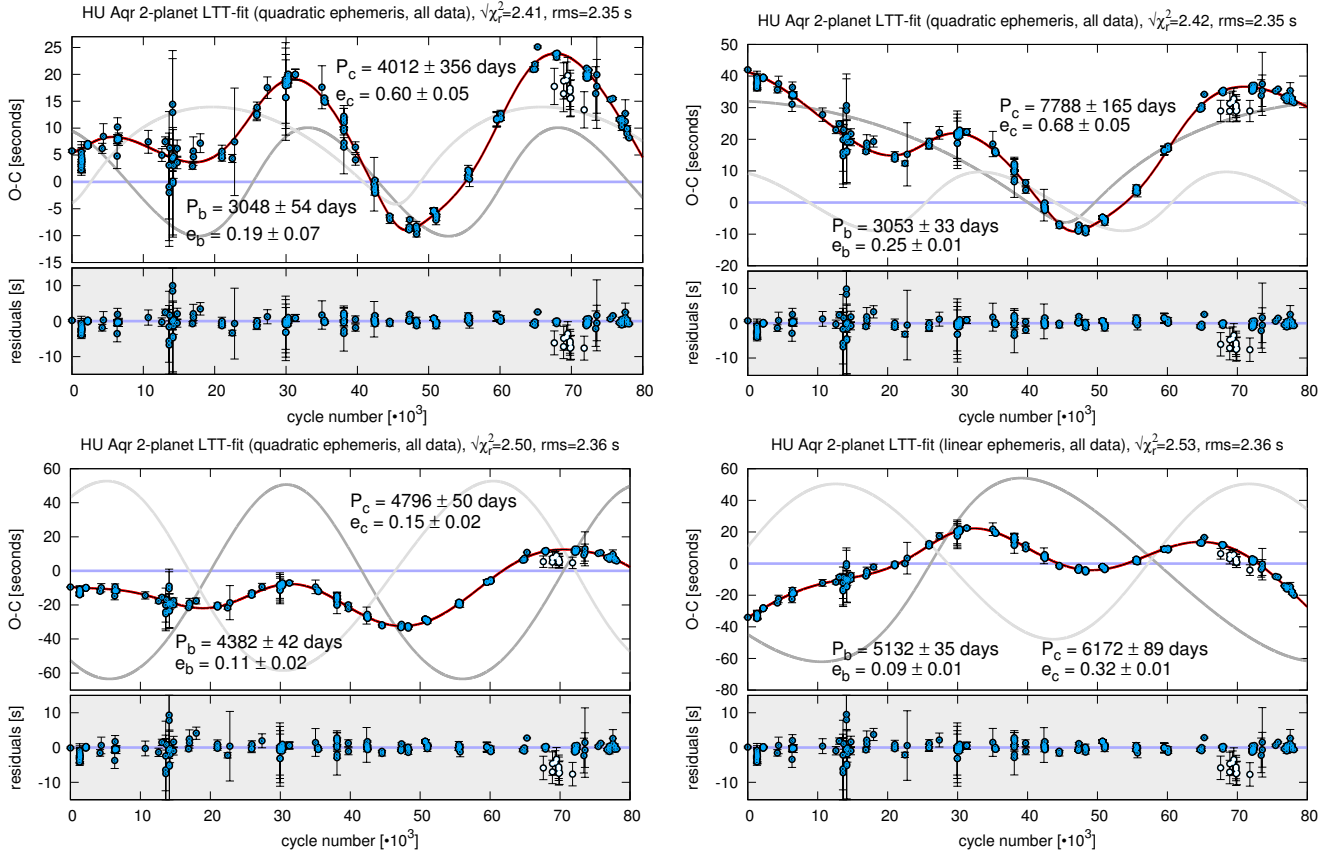


**Figure A2.** Examples of synthetic curves of the 2-planet LTT quadratic and linear (*the bottom right panel*) ephemeris models to all 171 data points analysed in this work, including 10 data points in Qian et al. (2011) which are marked with white filled circles. The shaded curves represent single planetary signal terms, respectively.

stable models characterised by  $(\chi^2_r)^{1/2} < 3$  and an rms  $< 2.1$  (still better than for the best 2-planet kinematic models). These fits have well bounded  $a_b \sim 4$  AU and small eccentricities up to 0.4. However, the oscillating semi-major axis of the outer body is unconstrained and covers many low order mean motion resonances, between 3c:2b MMR and 5c:1b MMR. Figure A4 shows synthetic curves of two example solutions corresponding to the 3c:2b MMR

(the left panel) and for a model close to 3c:1b MMR (the right panel). To identify these resonances, in the neighborhoods of a few selected best fit models, we derived high-resolution dynamical maps (1440  $\times$  900 data points) shown in Fig. A5. These maps are computed in terms of the fast indicator MEGNO (Cincotta et al. 2003), with the help of our recently developed CPU cluster soft-

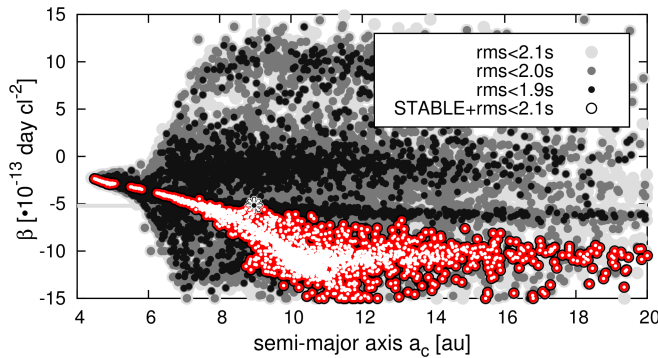


**Figure A6.** Statistics of 2-planet  $N$ -body quadratic ephemeris models gathered with the hybrid algorithm, projected onto the  $(a_c, \beta)$ -plane, for the quadratic ephemeris. Meaning of symbols is the same as in Fig. A3.

ware MECHANIC<sup>3</sup> (Słonina et al. 2012). MEGNO measures the maximal Lyapunov exponent, which makes it possible to distinguish between chaotic and regular solutions. Each point at these maps has been integrated over  $\sim 10^4$  orbital periods of the outermost companion. The dynamical maps confirm that the Lagrange stable models examined over a limited time-span are equivalent to quasi-periodic, stable solutions.

A solution illustrated in the left panel of Fig. A4 is the best-fit *stable* model found in the hybrid search with  $(\chi^2_{\nu})^{1/2} \sim 2.82$  and an  $\text{rms} \sim 2$  sec. It is located in a very narrow, isolated stability island of the 3c:2b MMR and characterised by relatively large  $\beta \sim -2.7 \times 10^{-13}$  day cycle<sup>-2</sup>, similarly to the kinematic model. The right panel of Fig. A4 shows a configuration close to the 3c:1b MMR, which has even larger  $\beta \sim -6 \times 10^{-13}$  day cycle<sup>-2</sup>.

Figure A6 shows a statistics of the best-fit solutions in the  $(a_c, \beta)$ -plane. It reveals that  $\beta$  is not constrained, regarding even its sign. Stable models exhibit a strong correlation between both these parameters. A larger value of the semi-major axis of the outer planet is related to a larger magnitude of  $\beta$ . Due to this correlation, an interpretation of stable configurations is complex. For relatively small magnitude of  $\beta$ , stable configurations are characterized by low order MMRs and may be found in tiny areas of stable motions (see Fig. A5). For more separated planets, when stability zones are much more extended,  $|\beta|$  increases. Already  $|\beta| \sim 2 \times 10^{-13}$  day cycle<sup>-2</sup> is difficult to explain by physical phenomena in the binary, as we discussed in Sect. 5. Such large values of  $|\beta|$  may indicate a third, long-period companion object in a very distant orbit. However, because already the 2-planet model is not constrained by the data, also a 3-planet configuration cannot be fixed without ambiguity. We did an attempt to search for such Newtonian 3-planet models within the linear ephemeris, but we did not find any improved, nor stable solutions of this type.

## REFERENCES

- Applegate J. H., 1992, *ApJ*, 385, 621  
 Bailes M., Lyne A. G., Shemar S. L., 1991, *Nature*, 352, 311  
 Baluev R. V., 2011, *Celestial Mechanics and Dynamical Astronomy*, 111, 235

<sup>3</sup> <http://git.astru.umk.pl/projects/mechanic>

- Beard S. M., Vick A. J. A., Atkinson D., Dhillon V. S., Marsh T., McLay S., Stevenson M., Tierney C., 2002 Vol. 4848 of Society of Photo-Optical Instrumentation Engineers (SPIE) Conference Series, Ultracam camera control and data acquisition system. pp 218–229
- Berdyugina S. V., 2005, *Living Reviews in Solar Physics*, 2, 8
- Beuermann K., Buhlmann J., Diese J., Dreizler S., Hessman F. V., Husser T.-O., Miller G. F., Nickol N., Pons R., Ruhr D., Sch Müller H., Schwöpe A. D., Sorge T., Ulrichs L., Winget D. E., Winget K. I., 2011, *A&A*, 526, A53
- Beuermann K., Hessman F. V., Dreizler S., Marsh T. R., Parsons S. G., Winget D. E., Miller G. F., Schreiber M. R., Kley W., Dhillon V. S., Littlefair S. P., Copperwheat C. M., Hermes J. J., 2010, *A&A*, 521, L60
- Brinkworth C. S., Marsh T. R., Dhillon V. S., Knigge C., 2006, *MNRAS*, 365, 287
- Charbonneau P., 1995, *A&A Suppl.*, 101, 309
- Cincotta P. M., Giordano C. M., Simó C., 2003, *Physica D Non-linear Phenomena*, 182, 151
- Coles W., Hobbs G., Champion D. J., Manchester R. N., Verbiest J. P. W., 2011, *MNRAS*, 418, 561
- Dhillon V. S., et al., 2007, *MNRAS*, 378, 825
- Doyle L. R. e. a., 2011, *Science*, 333, 1602
- Eastman J., Siverd R., Gaudi B. S., 2010, *PASP*, 122, 935
- Goździewski K., Konacki M., 2004, *ApJ*, 610, 1093
- Goździewski K., Konacki M., Maciejewski A. J., 2003, *ApJ*, 594, 1019
- Goździewski K., Maciejewski A. J., 2001, *ApJL*, 563, L81
- Goździewski K., Migaszewski C., Musielniński A., 2008, in Y.-S. Sun, S. Ferraz-Mello, & J.-L. Zhou ed., *IAU Symposium Vol. 249 of IAU Symposium, Stability constraints in modeling of multi-planet extrasolar systems*. pp 447–460
- Hairer E., Nærsett S. P., Wanner G., 2009, *Solving Ordinary Differential Equations I: Nonstiff Problems*
- Hellier C., 2001, *Cataclysmic Variable Stars*
- Hilditch R. W., 2001, *An Introduction to Close Binary Stars*
- Hinse T. C., Lee J. W., Goździewski K., Haghighipour N., Lee C.-U., Scullion E. M., 2012, *MNRAS*, p. 2221
- Holmes S., Kolb U., Haswell C. A., Burwitz V., Lucas R. J., Rodriguez J., Rolfe S. M., Rostron J., Barker J., 2011, *PASP*, 123, 1177
- Horner J., Marshall J. P., Wittenmyer R. A., Tinney C. G., 2011, *MNRAS*, 416, L11
- Irwin J. B., 1952, *ApJ*, 116, 211
- Kanbach G., Kellner S., Schrey F. Z., Steinle H., Straubmeier C., Spruit H. C., 2003 Vol. 4841 of Society of Photo-Optical Instrumentation Engineers (SPIE) Conference Series, Design and results of the fast timing photo-polarimeter OPTIMA. pp 82–93
- Kanbach G., Stefanescu A., Duscha S., Mühlegger M., Schrey F., Steinle H., Slowikowska A., Spruit H., 2008 Vol. 351 of *Astrophysics and Space Science Library*, OPTIMA: A High Time Resolution Optical Photo-Polarimeter. pp 153–+
- Laughlin G., Chambers J. E., 2001, *ApJL*, 551, L109
- Lee J. W., Kim S.-L., Kim C.-H., Koch R. H., Lee C.-U., Kim H.-I., Park J.-H., 2009, *AJ*, 137, 3181
- Lee J. W., Lee C.-U., Kim S.-L., Kim H.-I., Park J.-H., 2011, *ArXiv e-prints*
- Lee M. H., Peale S. J., 2003, *ApJ*, 592, 1201
- Malhotra R., 1993, in J. A. Phillips, S. E. Thorsett, & S. R. Kulkarni ed., *Planets Around Pulsars Vol. 36 of Astronomical Society of the Pacific Conference Series, Orbital dynamics of PSR1257+12 and its two planetary companions*. pp 89–106

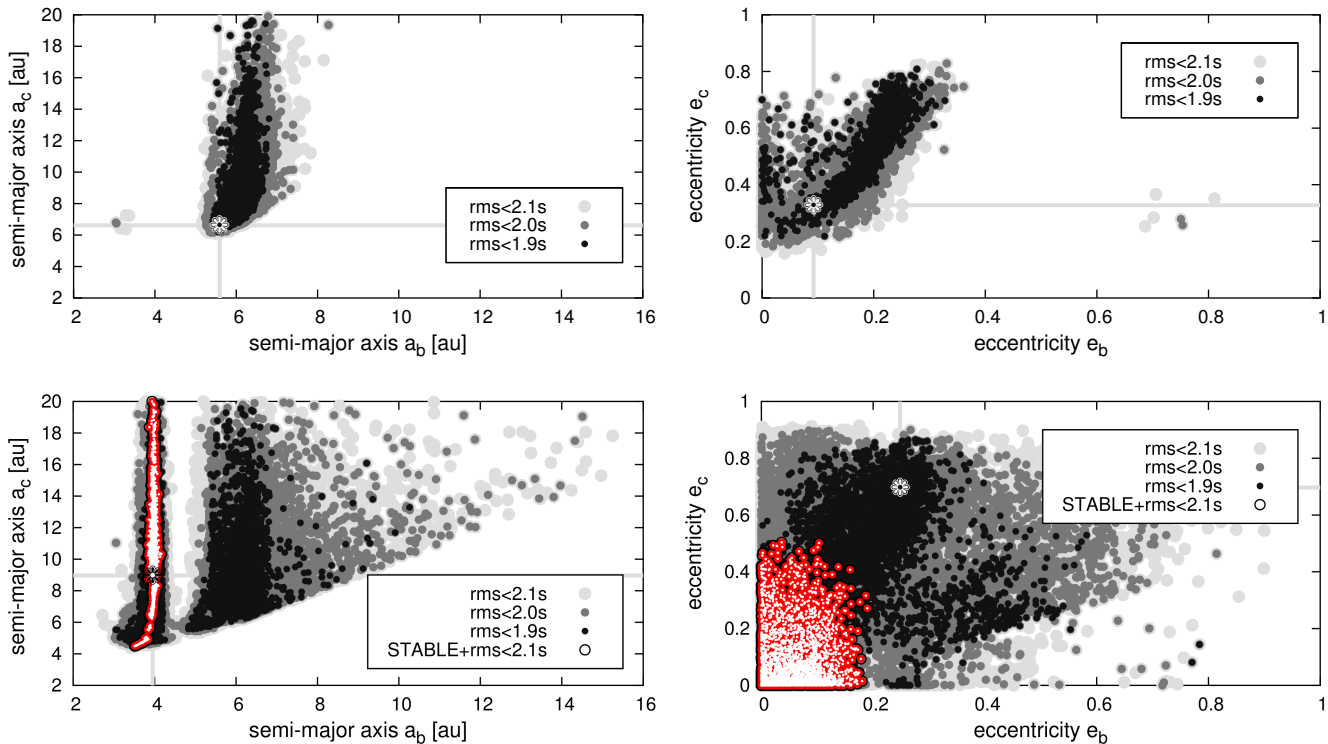


**Figure A3.** Statistics of 2-planet  $N$ -body models gathered with the hybrid algorithm, projected onto planes of selected parameters. *The top row* illustrates the results for the linear ephemeris, *the bottom row* shows the fits for the quadratic ephemeris model. The rms quality of these solutions is coded as filled circles: the better fit—the darker colour. Orbital parameters of the best-fit solutions are marked with shaded, intersecting lines and a flower symbol. Solutions Lagrange–stable over  $10^6$  revolutions of the outermost planet are marked with red–white circles.

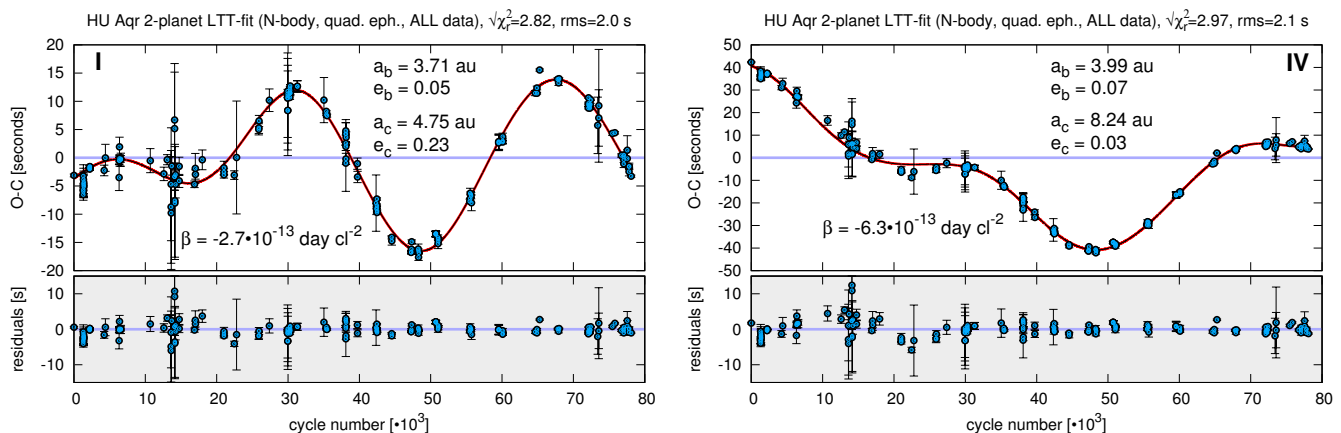


**Figure A4.** Examples of synthetic LTT curves and (O-C) residuals for *stable* 2-planet quadratic ephemeris Newtonian ( $N$ -body) models to 161 data points analysed in this work, without 10 data points in Qian et al. (2011). These models are selected from a sample illustrated in Fig. A3. Dynamical maps of these solutions shows Fig. A5 (they are labelled with the Roman numerals, as I and IV, respectively).

Morbidelli A., 2002, *Modern celestial mechanics : aspects of solar system dynamics*

Nasiroglu I., Slowikowska A., Kanbach G., Schwarz R., Schwöpe A. D., 2010, in *High Time Resolution Astrophysics (HTRA) IV - The Era of Extremely Large Telescopes Proceedings of Science, The orbital ephemeris of HU Aquarii observed with OPTIMA. Are there two giant planets in orbit?*

Pont F., Zucker S., Queloz D., 2006, *MNRAS*, 373, 231

Potter S. B., et al., 2011, *MNRAS*, 416, 2202

Press W. H., 2002, *Numerical recipes in C++ : the art of scientific computing*

Qian S.-B., Liu L., Liao W.-P., Li L.-J., Zhu L.-Y., Dai Z.-B., He J.-J., Zhao E.-G., Zhang J., Li K., 2011, *MNRAS*, 414, L16

Schwarz R., Schwöpe A. D., Vogel J., Dhillon V. S., Marsh T. R., Copperwheat C., Littlefair S. P., Kanbach G., 2009, *A&A*, 496, 833

Schwöpe A., et al., 2004, in S. Vrielmann & M. Cropper ed., *IAU Colloq. 190: Magnetic Cataclysmic Variables Vol. 315 of As-*

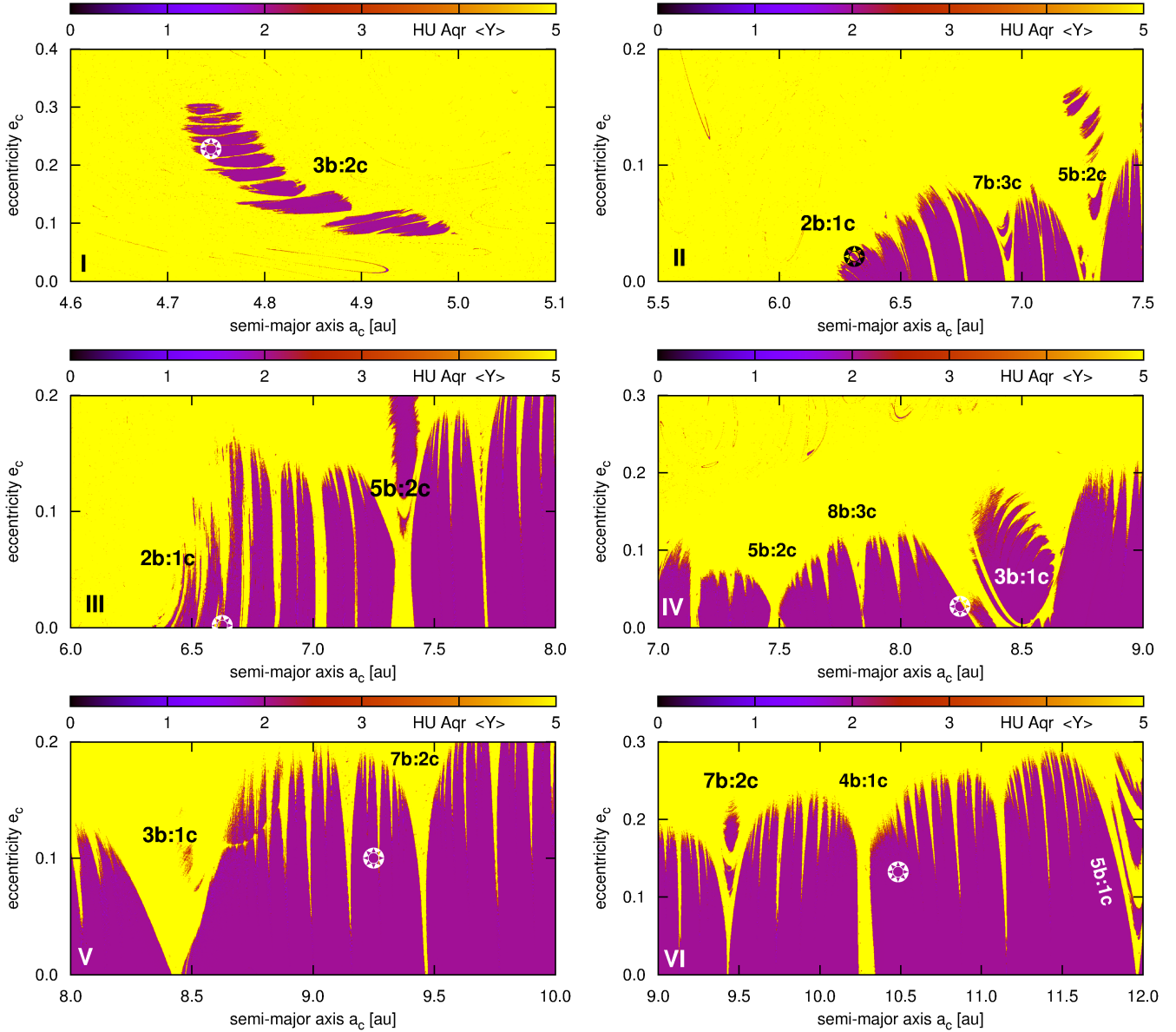


**Figure A5.** MEGNO dynamical maps in the  $(a_c, e_c)$ -plane for a few representative  $N$ -body *stable* solutions illustrated in the bottom panels of Fig. A4. Yellow colour encodes strongly unstable (chaotic) configurations, and purple colour (MEGNO  $\langle Y \rangle \sim 2$ ) is for stable, quasi-periodic solutions. Parameters of the nominal, tested fits are marked with the star symbol. The most prominent, low-order mean motion resonances are labeled. The original resolution of these dynamical maps is  $1440 \times 900$  data points integrated for  $10^4$  outermost orbital period each. The total mass of the binary is  $0.98 M_\odot$  (Schwope et al. 2011).

tronomical Society of the Pacific Conference Series, REVIEW: Multiwavelength Observations of eclipsing polars. p. 92  
 Schwope A. D., Horne K., Steeghs D., Still M., 2011, *A&A*, 531, A34  
 Schwope A. D., Schwarz R., Sirk M., Howell S. B., 2001, *A&A*, 375, 419  
 Słonińska M., Goździewski K., Migaszewski C., 2012, in F. Arenou & D. Hestroffer ed., *Orbital Couples: Pas de Deux in the Solar System and the Milky Way* (arXiv:1202.6513v1, in print)  
 Mechanic: a new numerical MPI framework for the dynamical astronomy  
 Tovmassian G. H., Zharikov S. V., Neustroev V. V., 2007, *ApJ*, 655, 466  
 Vogel J., 2008, PhD thesis, Technische Universität Berlin, Ger-

many  
 Vogel J., Schwope A., Schwarz R., Kanbach G., Dhillon V. S., Marsh T. R., 2008, in D. Phelan, O. Ryan, & A. Shearer ed., *High Time Resolution Astrophysics: The Universe at Sub-Second Timescales* Vol. 984 of American Institute of Physics Conference Series, On the orbital period of the magnetic cataclysmic variable HU Aquarii. pp 264–267  
 Warner B., 1995, *Cambridge Astrophysics Series*, 28  
 Welsh et al. 2012, *Nature*, doi:10.1038/nature10768 (in press), 1  
 Wittenmyer R. A., Horner J., Marshall J. P., Butters O. W., Tinney C. G., 2012, *MNRAS*, 419, 3258